

---

## Disclaimer

---

This manuscript has been submitted for consideration to NATURE GEOSCIENCE. Please note that the MS has not undergone peer review at this stage. Subsequent versions of this manuscript may have different content. If accepted, the final version of this manuscript will be available via the 'Peer-reviewed Publication DOI' link on the right-hand side of this webpage.

Please feel free to contact any of the authors with feedback and suggestions for improvements.

## Document history

---

Date	Action
1/Jul/2020	MS sent to co-authors for final draft acceptance
3/Jul/2020	IGSN for samples requested Spreadsheet and scripts submitted to Zenodo. MS Submitted to EarthArXiv

---

# AN EARLY PLIOCENE RELATIVE SEA LEVEL RECORD FROM PATAGONIA (ARGENTINA)

PREPRINT, COMPILED JULY 3, 2020

Alessio Rovere<sup>1</sup>, Marta Pappalardo<sup>2</sup>, Sebastian Richiano<sup>3</sup>, Marina Aguirre<sup>4</sup>, Michael R. Sandstrom<sup>5</sup>, Paul J. Hearty<sup>6</sup>,  
Jacqueline Austermann<sup>5</sup>, Ignacio Castellanos<sup>7</sup>, and Maureen E. Raymo<sup>5</sup>

<sup>1</sup>MARUM - Center for Marine Environmental Sciences, University of Bremen

<sup>2</sup>Department of Earth Sciences, Università degli studi di Pisa

<sup>3</sup>Instituto Patagónico de Geología y Paleontología, CONICET, Puerto Madryn

<sup>4</sup>CONICET, CCT-La Plata and Universidad Nacional de La Plata

<sup>5</sup>Lamont Doherty Earth Observatory, Columbia University

<sup>6</sup>Department of Geological Sciences, Jackson School of Geosciences, The University of Texas at Austin

<sup>7</sup>Baker Hughes

## ABSTRACT

We report a geological unit surveyed and dated in central Patagonia, Argentina (Camarones town, San Jorge Gulf). The unit was interpreted as representative of an intertidal environment and dated to the Early Pliocene (4.69-5.23 Ma) with strontium isotope stratigraphy. The elevation of this unit was measured with differential GPS at ca. 36 m above present-day sea level. Considering modern tidal ranges, it was possible to constrain paleo relative sea level within  $\pm 2.5\text{m}$  ( $1\sigma$ ). We use glacial isostatic adjustment models and estimates of vertical land movement to calculate that, when the Camarones intertidal sequence was deposited, global mean sea level was  $28.4 \pm 11.7\text{m}$  above present. This estimate matches those derived from analogous Early Pliocene sea level proxies in the Mediterranean Sea and South Africa. Evidence from these three locations indicates that Early Pliocene sea level may have exceeded 20m above its present level. Such high global mean sea level values imply an ice-free Greenland, a significant melting of West Antarctica, and a contribution of East Antarctica to global mean sea level.

**Keywords** Early Pliocene · Sea level · Stratigraphy

## 1 INTRODUCTION

The survey, interpretation and dating of paleo relative sea level (RSL) indicators (such as fossil coral reefs or relic beach deposits<sup>1</sup>) is paramount to constraining the maximum elevation reached by global mean sea level during periods of the Earth's history warmer than the pre-industrial. Once measured, observed paleo RSL indicators must be corrected for processes causing "Departures from Eustasy"<sup>2</sup> (such as tectonics, mantle dynamic topography, DT, and glacial isostatic adjustment, GIA<sup>3;4</sup>) the elevation of paleo RSL indicators is the only direct proxy available to estimate global mean sea level in Earth's past. These estimates are in turn important to informing models of ice sheet melting under future warmer climates<sup>5</sup>.

A recent global compilation by Khan et al., 2019<sup>6</sup> showed that more than 5000 RSL indicators globally span the last 30 ka. The number of surveyed RSL indicators is greatly reduced for older time periods: another compilation of Pleistocene RSL indicators<sup>7</sup> reports that more than 1000 Last Interglacial (MIS 5e, 125 ka) and only around 20 MIS 11 (400 ka) RSL indicators are preserved globally. Only a handful of sites exist that document sea level highstands beyond one million years ago<sup>2;8;9;10</sup>. In general, robust RSL indicators predating 400 ka are rare because they are poorly preserved and difficult to date with precision. Additionally, relating them to global mean sea level, GMSL, is difficult since they are likely affected by significant post-depositional movement. This limits our ability to gauge the sensitivity of ice caps to warmer climate conditions, such as those that characterized Earth in the Pliocene.

Some of the oldest, precisely dated and measured RSL indicators were recently surveyed on the island of Mallorca (Balearic Islands, Spain), in a coastal cave called "Coves d'Artá". Here, six phreatic overgrowths on speleothems mark the paleo water/air interface within the cave<sup>9</sup>, and are therefore closely related to paleo RSL. The highest and oldest of these formations was measured at  $31.8 \pm 0.25\text{m}$  above mean sea level, and yielded a U-Pb age of  $4.29 \pm 0.39\text{Ma}$  ( $2\sigma$ )<sup>9</sup>. Taking into account GIA and possible long-term deformation due to tectonics or dynamic topography, it was estimated that global mean sea level at the time of deposition of this RSL indicator was 25.1m above present, bounded by uncertainties represented by 16<sup>th</sup>-84<sup>th</sup> percentiles of 10.6-28.3m<sup>9</sup>. For the same time period, a second study<sup>10</sup> reported a site in the Republic of South Africa (Northern Cape Province, site Cliff Point, ZCP, Section2). Here, oyster shells living in a paleo subtidal to intertidal environment constrain paleo RSL at  $35.1 \pm 2.2\text{m}$  ( $1\sigma$ ). The oysters were dated to 4.28-4.87 Ma ( $2\sigma$  range) with strontium isotope stratigraphy (SIS). While paleo global mean sea level estimates were not calculated at this site, based on the Mallorca benchmark the authors argue that this location was affected by relatively minor vertical land movements (possibly uplift) since 5 Ma.

While indirect paleo sea level estimates spanning the last 5.3 Ma are available from oxygen isotopes<sup>12;13</sup>, the two studies cited above are arguably the only ones reporting relatively precise and well-dated direct sea-level observations for the Early Pliocene. This period coincides with the Pliocene Climatic Optimum, that is regarded as a past analogue for future warmer climate<sup>14</sup>. At this time, CO<sub>2</sub> was between pre-industrial and modern levels<sup>15</sup> and, during interglacials, average global temperatures were 2-

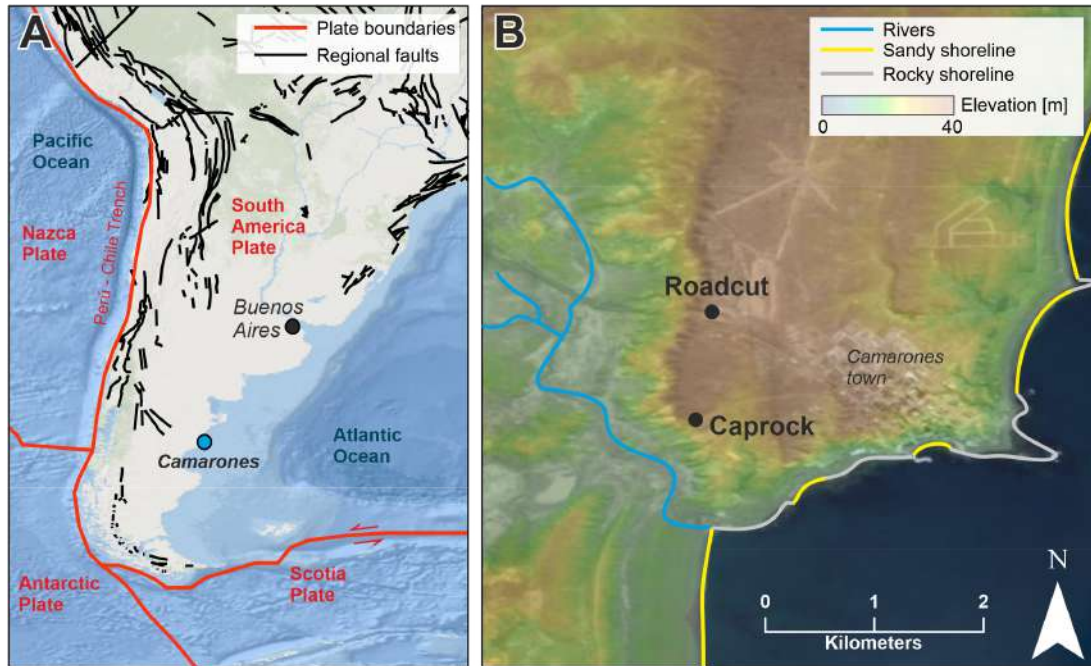


Figure 1: A) Location of the study area and main geological structures in the Southern part of South America. B) Topography of the Camarones town area, with location of the two outcrops (*Roadcut* and *Caprock*) presented in this study. Map sources: Esri, DigitalGlobe, GeoEye, Earthstar Geographics, CNES/Airbus DS, USDA, USGS, AeroGRID, IGN, DeLorme, GEBCO, NOAA NGDC, SRTM, the GIS User Community and other contributors. Elevation data in B are from the Shuttle Radar Topography Mission<sup>11</sup>

59 3°C higher than pre-industrial values<sup>16</sup>. Pliocene climate was  
 60 modulated by a ca. 40kyr periodicity in glacial/interglacial  
 61 cycles with highstands and lowstands that were characterized by  
 62 sea-level oscillations as high as  $13 \pm 5\text{m}$ <sup>17</sup>. Ice models suggest  
 63 that, during the warmest Pliocene interglacials, Greenland was  
 64 ice-free<sup>18</sup>. The West Antarctic Ice sheet was subject to periodic  
 65 collapses<sup>19</sup>, contributing as much as  $7\text{m}$ <sup>20</sup> to global mean sea  
 66 level. Ice models and field-based evidence<sup>21</sup> suggest that also  
 67 the East Antarctic Ice Sheet might have been smaller than today,  
 68 contributing another  $3\text{m}$ <sup>20</sup> to  $13\text{-}16\text{m}$ <sup>22</sup> to global mean sea level.

69 In this study, we report an Early Pliocene foreshore (intertidal)  
 70 sequence located in the town of Camarones, along the coast of  
 71 central Patagonia, Argentina (fig. 2). Combining field data, SIS  
 72 ages, GIA and DT models we conclude that this deposit formed  
 73  $4.69\text{-}5.23\text{Ma}$  ago ( $2\sigma$  range) when sea level was  $28.4 \pm 11.7$  ( $1\sigma$ )  
 74 higher than today. This estimate is broadly consistent with those  
 75 derived from the Republic of South Africa and Spain. Together,  
 76 these three studies present a consistent picture of global mean  
 77 sea level during the Pliocene Climatic Optimum that exceeded  
 78  $20\text{m}$  above modern sea level.

## 79 THE PLIOCENE SEA LEVEL RECORD AT CAMARONES, 80 CENTRAL PATAGONIA, ARGENTINA

81 The Patagonia geographic region includes territories belonging  
 82 to the states of Argentina and Chile. Geologically, Patagonia  
 83 represents the southernmost tip of the South American plate  
 84 (Figure 1A). Along the Pacific coasts of Patagonia, the Nazca  
 85 and the Antarctic plates are subducting below the Andes. To-  
 86 wards the south, the Scotia plate moves eastward and outlines

87 Tierra del Fuego, at South America's southern tip<sup>23</sup>. To the East,  
 88 the Patagonian Atlantic coast is a passive margin, tectonically  
 89 characterized as an extensional stress field and bordered by a  
 90 wide continental shelf. The central and eastern parts of this  
 91 landmass are represented by the Andean foreland, formed by  
 92 Palaeozoic-Mesozoic metamorphic basement overlapped by  
 93 Tertiary continental and marine sedimentary rocks, dating back  
 94 to the Paleocene. These are covered by Eocene–Oligocene py-  
 95 roclastic rocks and Middle Miocene fluvial sediments. Marine  
 96 sedimentary rocks corresponding to Tertiary transgressions are  
 97 located east of the Andean foreland<sup>24</sup>. In the Middle Miocene,  
 98 the Chile Triple Junction migrated northward, leading to the  
 99 opening of an asthenospheric window below southern Patagonia<sup>25</sup>.  
 100 This caused a switch from subsidence to uplift, and the  
 101 Patagonia region underwent a moderate but continuous uplift.<sup>26</sup>

102 Along the coastlines of Central Patagonia, several levels of paleo  
 103 shorelines above modern sea level were already noted by  
 104 Charles Darwin in his Beagle voyage<sup>27</sup>, and were the subject  
 105 of more than 150 years of research (see Supplementary Infor-  
 106 mation for details). Studies in Central Patagonia include coastal  
 107 sequences of Holocene<sup>28;29</sup>, Pleistocene<sup>30;31;32</sup> and Pliocene-  
 108 to-Miocene<sup>33;34</sup> age. Among the latter, Del Río et al<sup>34</sup> dated  
 109 Early Pliocene mollusks from marine deposits few hundreds of  
 110 kilometers south of the study area described in this study (see  
 111 Supplementary Information for details).

112 The town of Camarones lies at the northern tip of the San Jorge  
 113 Gulf, approximately  $1300\text{ km}$  south of Buenos Aires, the capi-  
 114 tal of Argentina. Within a few kilometers of Camarones, sev-  
 115 eral paleo-sea level indicators have been preserved, from the  
 116 Holocene<sup>35</sup> to the Pleistocene<sup>30</sup>. Already in the late 1940s, the



Figure 2: The *Roadcut* outcrop at Camarones. The inset shows a detail of Unit **Cp**, a shelly-rich layer interpreted as representative of a foreshore (intertidal) environment dating to the Early Pliocene. Each unit is described in details in the Supplementary Information, including descriptions of the *Caprock* outcrop.

117 Italian geologist Feruglio<sup>36</sup> identified an elevated marine terrace  
 118 along a roadcut carved on the main road leading into the  
 119 town of Camarones that he tentatively attributed to the Pliocene.  
 120 A recent study<sup>30</sup> confirmed the elevation of this terrace at ca.  
 121 40m above sea level, which is therefore located at the lower  
 122 bound of the "beach barriers and terrace deposits between 40  
 123 and 110m elevation" as reported in the 1:250.000 geological  
 124 chart of Camarones<sup>37</sup>.

125 Radiometric ages, precise GPS elevations and stratigraphic  
 126 descriptions of cross-sections surveyed along this so-called  
 127 High Terrace (originally named, in Spanish, *Teraza Alta de*  
 128 *Camarones*<sup>36</sup>) are the subject of this paper. Along this terrace,  
 129 we surveyed and dated samples from two sites, separated by less  
 130 than one kilometer. One is the *Roadcut*, already recognized and  
 131 described by Feruglio<sup>36</sup>. We did not find reports of the second  
 132 site (that we here call *Caprock*, Figure 1B) in the existing litera-  
 133 ture, although it is possible that it was included in the geological  
 134 description of the High Terrace by previous authors. At both  
 135 sites, we recognized a geological facies representative of sedi-  
 136 mentation in a foreshore environment (i.e. in the intertidal zone)  
 137 that marks paleo RSL with high accuracy. All data described  
 138 hereafter and in the Supplementary Information annexed to this  
 139 article is available in a spreadsheet uploaded to Zenodo<sup>38</sup>.

140 **Paleo RSL.** In general, *Roadcut* and *Caprock* represent sedi-  
 141 mentation during a transgressive event on top of a raised shore  
 142 platform (see Supplementary Information for details). Among  
 143 the units identified within the *Roadcut* (Figure 2), one (Unit **Cp**,  
 144 see inset in Figure 2) is composed of well-cemented fine con-  
 145 glomerates with rounded pebbles and shells. In particular, the  
 146 uppermost part of this unit contains a dense faunal assemblage  
 147 in the form of a shellbed, where we recognized 15 different

species of bivalves and 11 species of gastropods (see Supple- 148  
 mentary Information for details). The bivalve shells are mostly 149  
 intact and sometimes with paired valves (articulated), but not 150  
 in living position. This unit was interpreted as representative 151  
 of a foreshore environment, i.e. the intertidal zone. The same 152  
 unit has been identified at the *Caprock* section, at roughly the 153  
 same elevation. The elevation of Unit **Cp** was measured at two 154  
 points at both *Roadcut* and *Caprock* (Table 1). From these mea- 155  
 surements, we calculate that Unit **Cp** has an **average elevation** 156  
**of  $36.2 \pm 0.5\text{m}$  ( $1\sigma$ )** above the GEOIDEAR16 geoid<sup>39</sup>, which 157  
 approximates present sea level. Using modern tidal values<sup>35</sup>, 158  
 and assuming no post-depositional movement, we calculate that 159  
 the two outcrops in the area of Camarones are indicative of a 160  
**paleo RSL at  $36.2 \pm 2.5\text{m}$  ( $1\sigma$ )** above present (see Methods for 161  
 details). 162

**Age.** Three oyster shells from *Roadcut* and *Caprock* were 163  
 analyzed by Strontium Isotope Stratigraphy (SIS) relative dating 164  
 techniques. Using sequential leaching to target the least altered 165  
 inner carbonate of each shell (Sandstrom et al., under review), 166  
 we obtained multiple SIS ages on three different shells (one 167  
 from *Caprock* and two from *Roadcut*). The shells yielded an 168  
 age range of  **$4.69\text{-}5.23\text{Ma}$**  ( $n=6$ ,  $2\sigma S_{EM}$ ) (see Methods and 169  
 Supplementary Information for details). 170

**Glacial Isostatic Adjustment.** The Early Pliocene intertidal 171  
 units surveyed at Camarones were subject to processes that 172  
 caused their past and current elevation to depart from eustasy. 173  
 These processes must be accounted for in order to reconstruct 174  
 global mean sea level at the time of formation. We calculate 175  
 Glacial Isostatic Adjustment (GIA) using 36 different Earth 176  
 models. For this site, we calculate a GIA correction of  $-14.6 \pm 3.2\text{m}$  177  
 ( $1\sigma$ ) (see Methods for details). This value is subtracted from the 178

179 observed paleo RSL and the uncertainty propagated. This correction is a combination of effects associated with the ongoing  
 180 response to the last deglaciation and Antarctic ice sheet oscillations during the early Pliocene<sup>2</sup>. The former contribution is  
 181  $-9.5 \pm 3\text{m}$  ( $1\sigma$ ), which means that the Argentinian coast today experiences sea level fall due to a combination of effects associated  
 182 with postglacial rebound due to the melting of the glacial Patagonian ice sheet as well as continental levering, ocean sy-  
 183 phoning, and rotational effects. Once fully relaxed, sea level at Camarones will therefore be lower (and a paleo sea level indicator higher) by approximately 9.5m than it is today. The addi-  
 184 tional contribution of  $\sim -5\text{m}$  is associated with the adjustment to 40kyr oscillations in the Antarctic ice sheet. The result is that,  
 185 at Camarones, **GIA-corrected paleo RSL is  $50.8 \pm 4.1\text{m}$  ( $1\sigma$ )**.

193 **Vertical Land Motions.** The GIA-corrected RSL elevation reported above needs to be further corrected for Vertical Land  
 194 Motions (VLMs), that can be either due to crustal tectonics, mantle dynamic topography<sup>40;41</sup> or deformation associated with  
 195 sediment loading/unloading<sup>42;43</sup>. As briefly outlined in the previous sections, Camarones is located on a passive margin, likely  
 196 subject to limited tectonic influence (see Supplementary Information for details). Dynamic topography models suggest that,  
 197 since MIS 5e (125 ka), the area of Camarones was subject to uplift, with rates increasing towards the South<sup>3</sup>. This is in  
 198 line with observations of much higher Pliocene shorelines (70-170m above sea level<sup>34</sup>) at locations 300-500 kilometers south  
 199 of Camarones (see Supplementary Information for details). A long-term slight uplift trend is also predicted by the models of  
 200 Flament et al., 2015<sup>44</sup> and Müller et al., 2018<sup>45</sup>. Predictions in these DT models average to  $4.5 \pm 2.2\text{m/Ma}$  (Table 3). Accounting  
 201 for the age of the deposit, this leads to a downward correction of our global mean sea level inference by  $22.5 \pm 11.0\text{m}$  ( $1\sigma$ ).  
 202 As is apparent from the variation of estimates for the dynamic topography rate, this correction remains quite uncertain and the  
 203 true value can possibly be even outside of this range given that it is difficult to fully explore model uncertainties.

215 **Global Mean Sea Level.** Using the value of VLM reported above and propagating the uncertainties related to RSL, GIA and  
 216 VLM, we calculate that, at the time of deposition of the *Caprock* and *Roadcut* outcrops, **global mean sea level was  $28.4 \pm 11.7\text{m}$**   
 217 **( $1\sigma$ )**. We remark that there are large unknowns associated with this value. First, as described above, dynamic topography re-  
 218 mains to be a process that has high uncertainties that are generally not fully quantified. Second, it is possible that, as it is the  
 219 case for the US Atlantic Coastal Plain<sup>42</sup>, flexural response to sediment loading or tectonic deformation (that are not consid-  
 220 ered here) could also contribute to further vertical land motions in this area.

## 227 EARLY PLIOCENE GLOBAL MEAN SEA LEVEL

228 Until recently, field evidence to support the answer to the question "How high was global mean sea level in the Early  
 229 Pliocene?" was elusive. A trilogy of independent lines of evidence is now available to answer this question. The age of the  
 230 outcrops reported in this paper overlap with recently published data from Spain<sup>9</sup> and South Africa<sup>10</sup> (Figure 3A). The common  
 231 denominator to these three sites is that they all report precise

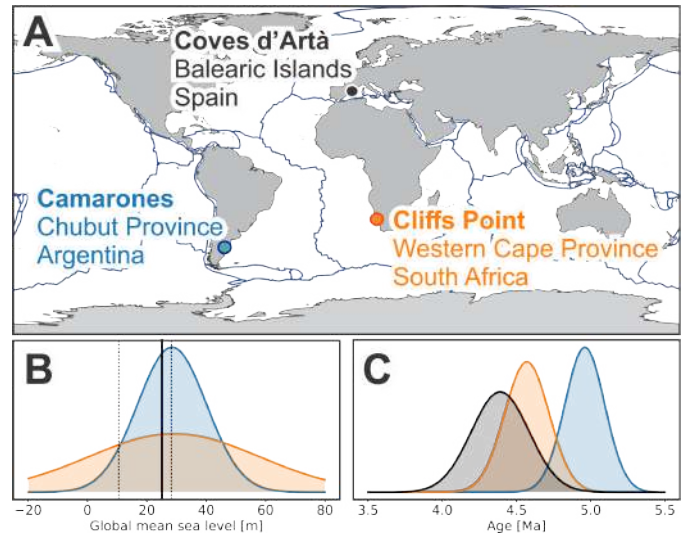


Figure 3: A) Location of Early Pliocene RSL indicators discussed in the text. Plate boundaries are shown in dark blue for reference. Background global map from GSHHS<sup>46</sup>, plate boundaries from Bird, 2003<sup>47</sup>. B) Global Mean Sea Level (GMSL) estimates for: i) Coves d'Artà (Balearic Islands, Spain), solid black line represents 16<sup>th</sup> percentile (25.1m), dotted black lines the 16<sup>th</sup>-84 percentiles<sup>9</sup>; ii) Camarones (Chubut Province, Argentina), blue normal distribution as described here ( $28.4 \pm 11.7\text{m}$ ,  $1\sigma$ ); iii) Cliffs Point (Northern Cape Province, South Africa), orange normal distribution as calculated from data in Hearty et al., 2020<sup>10</sup>, corrected with the same GIA and DT models used for Camarones ( $29.1 \pm 29\text{m}$ ,  $1\sigma$ ). C) Age estimates for Coves d'Artà (black), Camarones (blue) and Cliffs Point (Orange). The python scripts to produce panels B and C is available via Zenodo<sup>48</sup>.

and well-dated RSL indicators and have been subject to minor or mild uplift.

While uncertainties in the estimated vertical land motions necessarily lead to large uncertainties in the global mean sea level estimates, there is overlap between the calculated global mean sea levels for Camarones ( $28.4 \pm 11.7\text{m}$ ,  $1\sigma$ ) and Coves d'Artà (25.1m, with 16<sup>th</sup>-84<sup>th</sup> percentiles of 10.6-28.3m, Figure 3B).

An estimate of global mean sea level from the proxy record at Cliffs Point, South Africa<sup>10</sup> is characterized by greater uncertainty. Corrected with the same GIA models used for Camarones (Table 2), this data point indicates a paleo RSL at  $44.7 \pm 2.7\text{m}$  ( $1\sigma$ ). The same DT models used at Camarones indicate possible uplift of  $3.4 \pm 6.3\text{m/Ma}$  ( $1\sigma$ ). This results in an average global mean sea level estimate that aligns with that from Camarones, but bounded by very large uncertainties (Figure 3B).

Despite the relevant uncertainties, the average global mean sea level calculated from the geological facies reported in Argentina (this study), South Africa<sup>10</sup> and Spain<sup>9</sup> is well above modern sea level. In each area, post-depositional uplift contributes significant uncertainties to these estimates. We remark that, within each of these broader regions, there are other well-constrained Plio-Pleistocene sea level index points that may eventually provide a better calibration for modeled uplift rates.

258 The fact that locations on three continents and of comparable  
 259 age give such similar estimates for paleo-RSL increases our confidence  
 260 in stating that global mean sea level during the Pliocene  
 261 Climatic Optimum likely exceeded 20m above present-day. This  
 262 conclusion would most likely require an ice-free Greenland, a  
 263 significantly melted West Antarctic Ice Sheet and a significant  
 264 contribution from the East Antarctic Ice Sheet. These results  
 265 can serve as an important calibration target for ice sheet modeling  
 266 and, of even more obvious concern, imply that the polar ice sheets  
 267 will not be immune to the impacts of ongoing global warming  
 268

269 **METHODS**

270 **Elevation measurements and paleo RSL estimates.** We  
 271 measured elevations with a high-precision differential GPS  
 272 system (Trimble ProXRT receiver and Trimble Tornado antenna)  
 273 equipped to receive OmniSTAR HP real-time corrections.  
 274 These corrections, in optimal conditions, allow to measure the  
 275 elevation of a point with an accuracy of 0.1-0.6 m (2 $\sigma$ ),  
 276 depending on the survey conditions. We remark that, while  
 277 at the *Caprock* outcrop there is a free view of the sky, at  
 278 the *Roadcut* satellite reception is hindered by the vertical  
 279 cliff face. This could explain, in part, the discrepancy in  
 280 the two points collected at this outcrop at relatively short  
 281 distance from each other. Data were originally recorded  
 282 in geographic WGS84 coordinates and in height above the  
 283 ITRF2008 ellipsoid. For each GPS point, we calculated heights  
 284 above Mean Sea Level (orthometric height) subtracting from  
 285 the measured ITRF2008 ellipsoid height the GEOIDEAR16  
 286 geoid height<sup>39</sup>. These geoidal elevations are the best available  
 287 approximation of mean sea level in this area. GEOIDEAR16  
 288 was estimated to have an overall accuracy of 10 cm  
 289 (<https://www.ign.gov.ar/NuestrasActividades/Geodesia/Geoide-Ar16>).  
 290 The location and elevations of Unit **Cp** at *Roadcut* and  
 291 *Caprock* are reported in Table 1. On average, we calculate that  
 292 the elevation of Unit **Cp** is 36.2  $\pm$  0.5m (1 $\sigma$ ).

Table 1: GPS position and elevation of Unit **Cp** measured at the *Roadcut* and *Caprock* sites. Lat/Lon are in WGS84 coordinates, Ellipsoid heights are referred to the ITRF08 ellipsoid, geoid heights to the GEOIDEAR16 geoid model.

Longitude (dec.degrees E)	Latitude (dec.degrees N)	Ellipsoid Height Height (m)	Elev. above geoid (m)	Elev. error 1 $\sigma$ (m)
<b>Roadcut</b>				
-65.727604	-44.790083	49.67	36.8	0.06
-65.727619	-44.790069	47.68	34.8	0.3
<b>Caprock</b>				
-65.728221	-44.799297	49.40	36.5	0.2
-65.728221	-44.799298	49.64	36.8	0.1
Average			<b>36.2</b>	<b>0.5</b>

293 The Unit **Cp** at the *Roadcut* and *Caprock* sites has been interpreted  
 294 as forming in the foreshore zone, i.e., in the intertidal zone. This means  
 295 that its indicative meaning<sup>49</sup> spans from Mean Lower Low Water (MLLW)  
 296 to Mean Higher High Water

(MHHW). Based on predicted tidal data for the harbour of Camarones  
 (link), Bini et al.<sup>35</sup> report that the maximum tidal range (MHHW to MLLW)  
 in Camarones is 5m. Using this value and the formulas described in Rovere  
 et al., 2016<sup>1</sup>, we calculate that paleo RSL associated with Unit **Cp** is  
 36.2  $\pm$  2.5m. We highlight that this value does not take into account  
 the possibility that, 5 Ma ago, tidal ranges were different than present-day  
 ones, due to different shelf bathymetry under higher sea levels<sup>50</sup>.

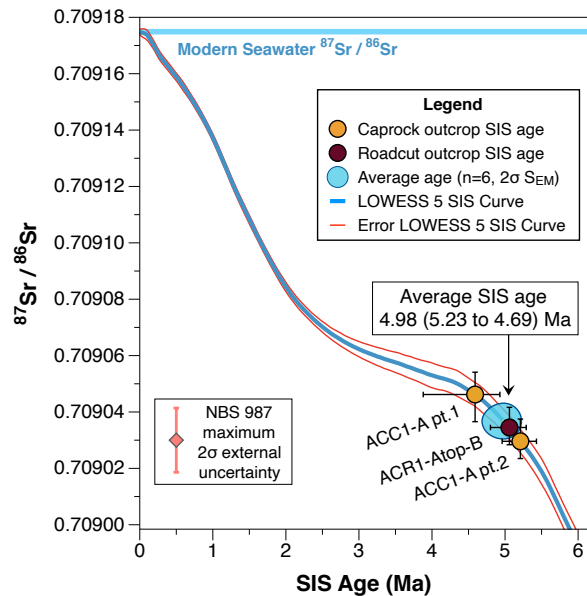


Figure 4: Sr isotope stratigraphy relative ages of oyster shells plotted on the SIS curve (LOWESS version 5)<sup>51</sup>. Orange points are from two separate portions of a shell from the *Caprock*, while maroon point is of a shell from unit **Cp** in the *Roadcut*. The average SIS age based on these samples is shown as a blue ellipse. Only inner leaches on the best-preserved specimens are shown. For the full dataset, see the Supplementary Information annexed to this paper. Modern seawater <sup>87</sup>Sr/<sup>86</sup>Sr values shown in light blue line. Maximum 2 $\sigma$  external uncertainty for the Sr isotope external standard NBS 987 is shown as red point for comparison (see Methods for details).

**Strontium Isotope Stratigraphy ages.** To attribute an age to Unit **Cp**, we used the Strontium Isotope Stratigraphy (SIS) curve published by McArthur et al. (2012)<sup>51</sup> (LOWESS version 5). Sr isotope ratios from carbonates are susceptible to post-depositional alteration, therefore, any significant reworking of Sr isotopes needs to be detected and discarded. Information on shell preservation was determined using <sup>87</sup>Sr/<sup>86</sup>Sr measurements on sequentially leached shell material (assuming smaller Sr isotope variations between leaches implies better preservation<sup>52;53</sup>) alongside standard screening techniques<sup>34;54</sup> and elemental analysis<sup>55;56</sup>. A preservation index between "1" (unaltered) and "3" (highly altered) was established for each sample based on these criteria (see Supplementary Information for details) with samples scoring above "2.0" excluded from results (see Hearty et al., 2020<sup>10</sup> and Sandstrom et al., under rev. for details).

We selected Ostreidae species for SIS chronological constraints, primarily because these shells precipitate original calcite mineral phases, making them more robust to diagenesis than arag-

323 onitic shells. Sample screening and chemical processing was  
 324 carried out at Lamont Doherty Earth Observatory (LDEO), and  
 325 all  $^{87}\text{Sr}/^{86}\text{Sr}$  measurements were made using Thermal Ion Mass  
 326 Spectrometry (TIMS) on an IsotopX Phoenix at SUNY Stony-  
 327 brook University (SBU) or a Finnigan Triton Plus at Lamont  
 328 Doherty Earth Observatory (LDEO).

329 We measured three oyster shells, one from the *Caprock* and two  
 330 from the *Roadcut* unit. The *Caprock* oyster (ACC1-A) was sam-  
 331 pled in three different locations, with inner leaches measured  
 332 on two of those splits, returning SIS ages of 4.59Ma (3.88 to  
 333 4.93Ma) and 5.21Ma (4.96 to 5.44Ma) (Figure 4). The third  
 334 sampling location was only measured for full dissolution, with  
 335 an average SIS age of 4.65Ma (4.42 to 4.83Ma), but provided  
 336 confidence in the shell Sr isotope heterogeneity and validated  
 337 analytical uncertainties (see Supplementary Information for de-  
 338 tails). The preservation index score for the caprock oyster(pt.1)  
 339 was 1.92. The two shells measured from the *Roadcut* (ACR1-  
 340 Atop-B and ACR1-Ctop-C) had inner leach SIS ages of 5.06Ma  
 341 (4.80 to 5.28Ma) (see Methods and Supplementary Information  
 342 for details), and 6.35Ma (6.19 to 6.53Ma), respectively. Addi-  
 343 tional diagenesis screening techniques on these shells included  
 344 elemental analysis (see Supplementary Information for details),  
 345 and variation of  $^{87}\text{Sr}/^{86}\text{Sr}$  within the leach set of each sample.  
 346 The results of sample variation compared to the inner leach  
 347  $^{87}\text{Sr}/^{86}\text{Sr}$  are shown in the Supplementary Information, with low  
 348 Sr isotope variation indicative of better preservation. Samples  
 349 with low variation tend to exhibit more radiogenic  $^{87}\text{Sr}/^{86}\text{Sr}$  val-  
 350 ues. Sample ACR1-Atop-B had a preservation index of 1.56,  
 351 while ACR1-Ctop-C had a score of 2.33 (see Supplementary  
 352 Information for details). Based on these screening criteria, we  
 353 exclude sample ACR1-Ctop-C, which appeared to have been  
 354 altered by low  $^{87}\text{Sr}/^{86}\text{Sr}$  fluids (possibly of through leaching  
 355 of surrounding volcanic material from the Complejo Marifil<sup>37</sup>).  
 356 The remaining inner leaches that passed screening were aver-  
 357 aged by filament to obtain an age of 4.98  $\pm$  0.245/-0.295Ma  
 358 ( $n=6$ ,  $2\sigma$  SEM) (see Methods and Supplementary Information  
 359 for details). In the text, this age is reported as a  $2\sigma$  range, i.e.,  
 360 4.69-5.23Ma.

361 **Glacial Isostatic Adjustment.** To account for changes in ver-  
 362 tical displacement and gravity field caused by GIA we use a  
 363 gravitationally self-consistent sea level model, that accounts  
 364 for the migration of shorelines and feedback of Earth's rota-  
 365 tion axis<sup>57</sup>. We compute both the contribution to GIA from  
 366 the amount of residual deformation caused by the most recent  
 367 Pleistocene glacial cycles and from ice age cycles during the  
 368 Pliocene.

369 For the first contribution we use the results from Raymo et al.<sup>2</sup>,  
 370 who calculated the residual deformation associated with the ice  
 371 model ICE-5G<sup>58</sup>. This ice history is paired with a suite of 36  
 372 different earth models with varying lithospheric thickness (48km,  
 373 71km, and 96km), upper and lower mantle viscosities ( $3 \times 10^{20}$   
 374 and  $5 \times 10^{20}$  Pa s for the upper mantle, and  $3 \times 10^{21}$  -  $30 \times 10^{21}$   
 375 for the lower mantle) to calculate a mean and standard deviation in  
 376 residual deformation (Figure 5).

377 For the second contribution we follow the approach described in  
 378 Dumitru et al.<sup>9</sup> by estimating ice mass variability based on the  
 379 benthic stack<sup>59</sup>. Following Miller et al.<sup>60</sup> we prescribe that 75%  
 380 of the benthic  $\delta^{18}\text{O}$  variability is due to ice volume changes (the

rest being due to temperature) and a further scaling of  $0.11\text{‰}/$   
 10m to convert  $\delta^{18}\text{O}_{\text{seawater}}$  into ice volume changes. These con-  
 382 versions are highly uncertain<sup>61;62</sup>, which highlights the need to  
 383 obtain local sea level based ice volume estimates. Nonetheless,  
 384 this scaling was used because it yielded comparable ice volume  
 385 estimates to the results of Dumitru et al.<sup>9</sup>. To construct an ice  
 386 history following this ice volume curve we only assume changes  
 387 in Antarctic ice volume given evidence that continent wide ex-  
 388 pansion of northern hemisphere ice sheets did only start around  
 389 3.3 Ma<sup>63</sup>. However, we acknowledge that an earlier intermittent  
 390 Greenland ice sheet might have existed<sup>64</sup>. We compute glacial  
 391 isostatic adjustment using this ice history and the same suite  
 392 of 36 different earth models described above. We extract local  
 393 predictions of relative sea level for Argentina, Mallorca, and  
 394 South Africa. To calculate global mean sea level changes we  
 395 integrate the amount of water in the ocean basins as a function of  
 396 time. We next calculate how this quantity has changed relative  
 397 to the initial state and divide it by the oceanic area calculated at  
 398 each time.  
 399

Note that this setup to calculate the GIA correction deviates  
 400 slightly from the one described in Dumitru et al.<sup>9</sup> in three small  
 401 ways, (1) we only consider one GMSL history for the Pliocene  
 402 rather than a range of histories, (2) we only consider variability  
 403 in southern hemisphere ice sheets and (3) we calculated GMSL  
 404 as described above rather than as changes in grounded ice vol-  
 405 ume.  
 406

The GIA corrections from both processes are combined. In a  
 407 last step we consider the age range for each sea level indicator  
 408 and average the GIA correction during warm periods, which we  
 409 define as times that had higher than average sea level over this  
 410 time period<sup>9</sup>. The mean and standard deviation that is obtained  
 411 is shown in table 2. We also show the GIA correction calculated  
 412 in<sup>9</sup> and note that the difference in mean GIA estimates stems  
 413 mostly from our different definition of global mean sea level.  
 414 For the analysis in the main text we use the GIA correction  
 415 described in<sup>9</sup> for the datapoint on Mallorca and not the one  
 416 recalculated here.  
 417

Table 2: GIA correction for Pliocene sea level markers at the  
 three locations discussed in the text. For comparison, we also  
 report the results for Mallorca used in Dumitru et al.<sup>9</sup>.

Location	Longitude	Latitude	mean GIA (m)	Stdev GIA (m)
Argentina	65.73° E	44.79° S	-14.6	3.2
South Africa	18.12° W	31.59° S	-9.6	1.6
Mallorca	3.45° W	39.66° N	2.9	2.2
Mallorca <sup>9</sup>	3.45° W	39.66° N	1.3	3.1

418 **Vertical Land Motions.** VLMs were extracted from pub-  
 419 lished Dynamic Topography models<sup>44;45</sup> using the Gplates portal  
 420 (<http://portal.gplates.org/>). The values extracted are reported in  
 421 Table 3. Flament et al.<sup>44</sup> focus on the surface expression of  
 422 subduction dynamics in South America. Their results are based  
 423 on forward advection modeling with different tectonic surface  
 424 boundary conditions. The different cases are based on different  
 425 timings of slab flattening. Müller et al.<sup>45</sup> have a global focus and  
 426 combine back advection (initialized with a seismic tomography

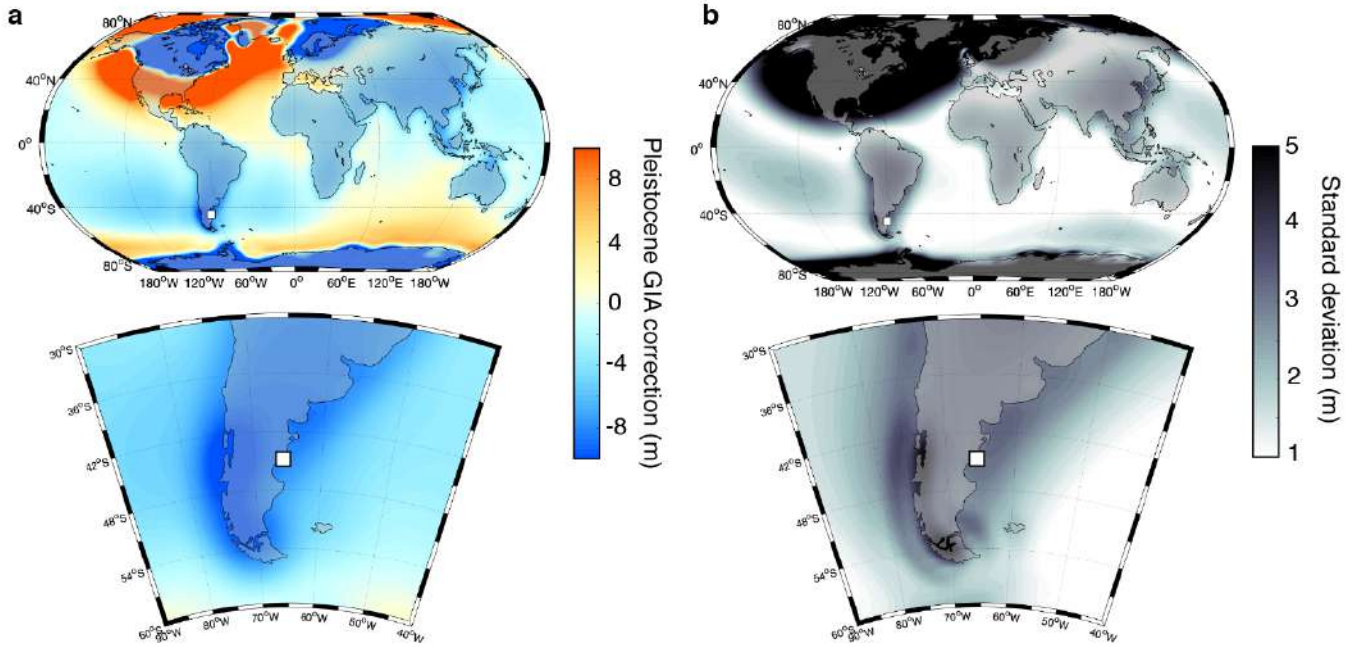


Figure 5: GIA contribution due to ongoing adjustment. The maps show the GIA contribution caused by the incomplete present-day adjustment to the late Pleistocene ice and ocean loading cycles. **a)** Model simulation using a viscosity structure of  $5 \times 10^{20}$  Pa s viscosity in the upper mantle,  $5 \times 10^{21}$  Pa s viscosity in the lower mantle, and an elastic lithospheric thickness of 96 km. **b)** Standard deviation of model predictions obtained using 36 different radial viscosity profiles, including varying the lithospheric thickness. The square in all insets marks the position of Camarones.

427 model) and forward advection with tectonic surface boundary  
 428 conditions. Their different models are based on different surface  
 429 plate reconstructions and different viscosity profiles.

Table 3: Amount of Vertical Land Motion (VLM), timeframe and rates extracted from published dynamic topography models for Camarones.

Reference	Model	VLM (m)	Timing (Ma)	Rate (m/Ma)
Müller et al., 2018 <sup>45</sup>	M1	4.6	10	0.46
	M2	66.2	10	6.62
	M3	45.0	10	4.50
	M4	58.0	10	5.80
	M5	45.4	10	4.54
	M6	21.8	10	2.18
	M7	25.5	10	2.55
Flament et al., 2015 <sup>44</sup>	Case 1	35.7	5	7.14
	Case 2	37.6	5	7.52
	Case 3	22.9	5	4.58
	Case 4	18.6	5	3.73

ACKNOWLEDGMENTS

This research investigation was among the primary objectives of the PLIOMAX grant, NSF OCE-1202632 (PI MER and co-PI PJH). AR acknowledges the Institutional Strategy of the University of Bremen, German Excellence Initiative (ABPZuK-03/2014). MER acknowledges the additional support of the G. Unger Vetlesen Foundation. MA acknowledges the following projects: Agencia Nacional de Promoción Científica y Tecnológica (PICT 2006-468, PICT 2013-1298), CONICET (PIP 0080, 0372 and 0729), and Universidad Nacional de La Plata (PI N11/587 and N11/726). The authors acknowledge PALSEA for useful discussions during annual meetings. PALSEA is a working group of the International Union for Quaternary Sciences (INQUA) and Past Global Changes (PAGES), which in turn received support from the Swiss Academy of Sciences and the Chinese Academy of Sciences. We also acknowledge Karla Rubio Sandoval Zurisadai for comments on the final draft of the MS. The background maps in Figure 1 of this article were created using ArcGIS® software by Esri. ArcGIS® and ArcMap™ are the intellectual property of Esri and are used herein under license. Copyright© Esri. All rights reserved. For more information about Esri® software, please visit www.esri.com. Plate boundaries in Figure 1 and Figure 3 were downloaded from GitHub (https://github.com/fraxen/tectonicplates/blob/master/). We thank Hugo Ahlenius, Nordpil and Peter Bird for putting this dataset publicly available online. We thank the Instituto Geográfico Nacional (Ministerio de Defensa, Argentina) for making publicly available the GEOIDEAR16 geoid model, which in this study was retrieved from http://www.isgeoid.polimi.it/.

430  
431  
432  
433  
434  
435  
436  
437  
438  
439  
440  
441  
442  
443  
444  
445  
446  
447  
448  
449  
450  
451  
452  
453  
454  
455  
456  
457  
458



## 459 AUTHOR CONTRIBUTIONS

460 AR, MP and SR wrote the MS and supplementary materials,  
 461 including figures. SR elaborated the stratigraphic description  
 462 of the Roadcut outcrop. MA provided expertise on the faunal  
 463 composition of the *Roadcut* and *Caprock* outcrops. MRS per-  
 464 formed SIS dating and contributed text on SIS methods and  
 465 results. JA produced GIA estimates, advised on DT and GMSL  
 466 calculations, and contributed to the writing of the paper. PJH  
 467 provided expertise on stratigraphic and geological interpretation  
 468 on the Camarones outcrops. All authors (except JA) participated  
 469 in different phases of the field expeditions to Camarones. IC  
 470 identified the *Caprock* site in the field. MER provided expertise  
 471 on the paleoclimatic implications of the study. All authors re-  
 472 visited the main text and Supplementary Information, and agree  
 473 with its contents.

## 474 REFERENCES

- 475 [1] Rovere, A. *et al.* The analysis of last interglacial (mis 5e)  
 476 relative sea-level indicators: Reconstructing sea-level in  
 477 a warmer world. *Earth-Science Reviews* **159**, 404–427  
 478 (2016).
- 479 [2] Raymo, M. E., Mitrovica, J. X., O’Leary, M. J., DeConto,  
 480 R. M. & Hearty, P. J. Departures from eustasy in pliocene  
 481 sea-level records. *Nature Geoscience* **4**, 328–332 (2011).
- 482 [3] Austermann, J., Mitrovica, J. X., Huybers, P. & Rovere,  
 483 A. Detection of a dynamic topography signal in last inter-  
 484 glacial sea-level records. *Science Advances* **3**, e1700457  
 485 (2017).
- 486 [4] Dutton, A. *et al.* Sea-level rise due to polar ice-sheet  
 487 mass loss during past warm periods. *science* **349**, aaa4019  
 488 (2015).
- 489 [5] DeConto, R. M. & Pollard, D. Contribution of antarctica to  
 490 past and future sea-level rise. *Nature* **531**, 591–597 (2016).
- 491 [6] Khan, N. S. *et al.* Inception of a global atlas of sea lev-  
 492 els since the last glacial maximum. *Quaternary Science*  
 493 *Reviews* **220**, 359–371 (2019).
- 494 [7] Pedroja, K. *et al.* Coastal staircase sequences reflecting sea-  
 495 level oscillations and tectonic uplift during the quaternary  
 496 and neogene. *Earth-Science Reviews* **132**, 13–38 (2014).
- 497 [8] Rovere, A. *et al.* The mid-pliocene sea-level conundrum:  
 498 Glacial isostasy, eustasy and dynamic topography. *Earth*  
 499 *and Planetary Science Letters* **387**, 27–33 (2014).
- 500 [9] Dumitru, O. A. *et al.* Constraints on global mean sea level  
 501 during pliocene warmth. *Nature* **574**, 233–236 (2019).
- 502 [10] Hearty, P. J. *et al.* Pliocene-pleistocene stratigraphy and  
 503 sea-level estimates, republic of south africa with implica-  
 504 tions for a 400 ppmv co2 world. *Paleoceanography and*  
 505 *Paleoclimatology* **n/a**, n/a (2020).
- 506 [11] USGS. Shuttle radar topography mission (srtm) 1 arc-  
 507 second global. *US Geological Survey* (2015).
- 508 [12] Rohling, E. *et al.* Sea-level and deep-sea-temperature  
 509 variability over the past 5.3 million years. *Nature* **508**,  
 510 477–482 (2014).
- 511 [13] Raymo, M. E., Kozdon, R., Evans, D., Lisiecki, L. & Ford,  
 512 H. L. The accuracy of mid-pliocene  $\delta^{18}O$ -based ice volume  
 and sea level reconstructions. *Earth-Science Reviews* **177**,  
 291–302 (2018).
- [14] Haywood, A. M. *et al.* Are there pre-quaternary geological  
 analogues for a future greenhouse warming? *Philosophical*  
*Transactions of the Royal Society A: Mathematical,*  
*Physical and Engineering Sciences* **369**, 933–956 (2011).
- [15] Fedorov, A. *et al.* Patterns and mechanisms of early  
 pliocene warmth. *Nature* **496**, 43–49 (2013).
- [16] Lunt, D. J. *et al.* Earth system sensitivity inferred from  
 pliocene modelling and data. *Nature Geoscience* **3**, 60–64  
 (2010).
- [17] Grant, G. *et al.* The amplitude and origin of sea-level  
 variability during the pliocene epoch. *Nature* **574**, 237–  
 241 (2019).
- [18] Solgaard, A. M., Reeh, N., Japsen, P. & Nielsen, T.  
 Snapshots of the greenland ice sheet configuration in the  
 pliocene to early pleistocene. *Journal of Glaciology* **57**,  
 871–880 (2011).
- [19] Naish, T. *et al.* Obliquity-paced pliocene west antarctic ice  
 sheet oscillations. *Nature* **458**, 322–328 (2009).
- [20] Pollard, D. & DeConto, R. M. Modelling west antarctic  
 ice sheet growth and collapse through the past five million  
 years. *Nature* **458**, 329–332 (2009).
- [21] Cook, C. P. *et al.* Dynamic behaviour of the east antarctic  
 ice sheet during pliocene warmth. *Nature Geoscience* **6**,  
 765–769 (2013).
- [22] Dolan, A. M. *et al.* Sensitivity of pliocene ice sheets  
 to orbital forcing. *Palaeogeography, Palaeoclimatology,*  
*Palaeoecology* **309**, 98–110 (2011).
- [23] Thomas, C., Livermore, R. & Pollitz, F. Motion of the  
 scotia sea plates. *Geophysical Journal International* **155**,  
 789–804 (2003).
- [24] Rabassa, J. Late cenozoic glaciations in patagonia and  
 tierra del fuego. *Developments in quaternary sciences* **11**,  
 151–204 (2008).
- [25] Guillaume, B., Martinod, J., Husson, L., Roddaz, M. &  
 Riquelme, R. Neogene uplift of central eastern patagonia:  
 Dynamic response to active spreading ridge subduction?  
*Tectonics* **28** (2009).
- [26] Ton-That, T., Singer, B., Mörner, N.-A. & Rabassa, J. Dat-  
 acción de lavas basálticas por 40ar/39ar y geología glacial  
 de la región del lago buenos aires, provincia de santa cruz,  
 argentina. *Revista de la Asociación Geológica Argentina*  
**54**, 333–352 (1999).
- [27] Darwin, C. *Geological observations on South America:*  
*Being the third part of the geology of the voyage of the*  
*Beagle, under the command of Capt. Fitzroy, RN during*  
*the years 1832 to 1836* (Smith, Elder and Company, 65,  
 Cornhill., 1846).
- [28] Schellmann, G. & Radtke, U. Coastal terraces and  
 holocene sea-level changes along the patagonian atlantic  
 coast. *Journal of Coastal Research* 983–996 (2003).
- [29] Zanchetta, G. *et al.* Middle-to late-holocene relative sea-  
 level changes at puerto deseado (patagonia, argentina). *The*  
*Holocene* **24**, 307–317 (2014).

- 568 [30] Pappalardo, M. *et al.* Coastal landscape evolution and  
569 sea-level change: A case study from central patagonia  
570 (argentina). *Zeitschrift für Geomorphologie* **59**, 145–172  
571 (2015).
- 572 [31] Rostami, K., Peltier, W. & Mangini, A. Quaternary marine  
573 terraces, sea-level changes and uplift history of patago-  
574 nia, argentina: comparisons with predictions of the ice-4g  
575 (vm2) model of the global process of glacial isostatic ad-  
576 justment. *Quaternary Science Reviews* **19**, 1495–1525  
577 (2000).
- 578 [32] Schellmann, G. & Radtke, U. ESR dating stratigraphically  
579 well-constrained marine terraces along the patagonian at-  
580 lantic coast (argentina). *Quaternary International* **68**, 261–  
581 273 (2000).
- 582 [33] Rutter, N. *et al.* Correlation and dating of quaternary  
583 littoral zones along the patagonian coast, argentina. *Qua-*  
584 *ternary Science Reviews* **8**, 213–234 (1989).
- 585 [34] Del Río, C., Griffin, M., McArthur, J., Martínez, S. &  
586 Thirlwall, M. Evidence for early pliocene and late miocene  
587 transgressions in southern patagonia (argentina): 87sr/86sr  
588 ages of the pectinid "chlamys" actinodes (sowerby). *Jour-*  
589 *nal of South American Earth Sciences* **47** (2013).
- 590 [35] Bini, M. *et al.* Mid-holocene relative sea-level changes  
591 along atlantic patagonia: new data from camarones, chubut,  
592 argentina. *The Holocene* **28**, 56–64 (2018).
- 593 [36] Feruglio, E. *Descripción geológica de la Patagonia*, vol. 1  
594 (Impr. y Casa Editora "Coni", 1949).
- 595 [37] Lema, H. A. *et al.* Hoja geológica 4566-ii y iv camarones  
596 (2001).
- 597 [38] Rovere, A. *et al.* Survey data, models and dated  
598 samples of the Pliocene shorelines of Camarones, Ar-  
599 gentina. (2020). URL [https://doi.org/10.5281/](https://doi.org/10.5281/zenodo.3929151)  
600 [zenodo.3929151](https://doi.org/10.5281/zenodo.3929151). Pre-review version.
- 601 [39] Piñón, D., Zhang, K., Wu, S. & Cimbaro, S. A new argen-  
602 tinean gravimetric geoid model: Geoideal. In *International*  
603 *Symposium on Earth and Environmental Sciences for Fu-*  
604 *ture Generations*, 53–62 (Springer, 2017).
- 605 [40] Braun, J. The many surface expressions of mantle dynam-  
606 ics. *Nature Geoscience* **3**, 825–833 (2010).
- 607 [41] Moucha, R. *et al.* Dynamic topography and long-term  
608 sea-level variations: There is no such thing as a stable  
609 continental platform. *Earth and Planetary Science Letters*  
610 **271**, 101–108 (2008).
- 611 [42] Moucha, R. & Ruetenik, G. A. Interplay between dynamic  
612 topography and flexure along the us atlantic passive margin:  
613 Insights from landscape evolution modeling. *Global and*  
614 *Planetary Change* **149**, 72–78 (2017).
- 615 [43] Ferrier, K. L., Austermann, J., Mitrovica, J. X. & Pico, T.  
616 Incorporating sediment compaction into a gravitationally  
617 self-consistent model for ice age sea-level change. *Geo-*  
618 *physical Journal International* **211**, 663–672 (2017).
- 619 [44] Flament, N., Gurnis, M., Müller, R. D., Bower, D. J. &  
620 Husson, L. Influence of subduction history on south amer-  
621 ican topography. *Earth and Planetary Science Letters* **430**,  
622 9–18 (2015).
- [45] Müller, R. D., Hassan, R., Gurnis, M., Flament, N. &  
Williams, S. E. Dynamic topography of passive conti-  
nental margins and their hinterlands since the Cretaceous.  
*Gondwana Research* **53**, 225–251 (2018).
- [46] Wessel, P. & Smith, W. H. A global, self-consistent, hi-  
erarchical, high-resolution shoreline database. *Journal*  
*of Geophysical Research: Solid Earth* **101**, 8741–8743  
(1996).
- [47] Bird, P. An updated digital model of plate boundaries.  
*Geochemistry, Geophysics, Geosystems* **4** (2003).
- [48] Rovere, A. Alerovere/paleo-sl-utilities 1.4 (2020). URL  
<https://doi.org/10.5281/zenodo.3929167>.
- [49] Shennan, I. Flandrian sea-level changes in the fenland. ii:  
Tendencies of sea-level movement, altitudinal changes, and  
local and regional factors. *Journal of Quaternary Science*  
**1**, 155–179 (1986).
- [50] Green, J., Huber, M., Waltham, D., Buzan, J. & Wells,  
M. Explicitly modelled deep-time tidal dissipation and its  
implication for lunar history. *Earth and Planetary Science*  
*Letters* **461**, 46–53 (2017).
- [51] McArthur, J., Howarth, R. & Shields, G. Strontium isotope  
stratigraphy. *The geologic time scale* **1**, 127–144 (2012).
- [52] Bailey, T., McArthur, J., Prince, H. & Thirlwall, M. Disso-  
lution methods for strontium isotope stratigraphy: whole  
rock analysis. *Chemical Geology* **167**, 313–319 (2000).
- [53] Li, D., Shields-Zhou, G. A., Ling, H.-F. & Thirlwall, M.  
Dissolution methods for strontium isotope stratigraphy:  
Guidelines for the use of bulk carbonate and phosphorite  
rocks. *Chemical Geology* **290**, 133–144 (2011).
- [54] McArthur, J. M. Recent trends in strontium isotope stratig-  
raphy. *Terra nova* **6**, 331–358 (1994).
- [55] Brand, U. & Veizer, J. Chemical diagenesis of a multicom-  
ponent carbonate system; 1, trace elements. *Journal of*  
*Sedimentary Research* **50**, 1219–1236 (1980).
- [56] Gothmann, A. M. *et al.* Fossil corals as an archive of  
secular variations in seawater chemistry since the mesozoic.  
*Geochimica et Cosmochimica Acta* **160**, 188–208 (2015).
- [57] Kendall, R. A., Mitrovica, J. X. & Milne, G. A. On post-  
glacial sea level–ii. numerical formulation and comparative  
results on spherically symmetric models. *Geophysical*  
*Journal International* **161**, 679–706 (2005).
- [58] Peltier, W. Global glacial isostasy and the surface of the  
ice-age earth: the ice-5g (vm2) model and grace. *Ann-*  
*ual Review of Earth and Planetary Sciences* **32**, 111–149  
(2004).
- [59] Lisiecki, L. E. & Raymo, M. E. A pliocene-pleistocene  
stack of 57 globally distributed benthic  $\delta^{18}O$  records. *Pa-*  
*leoceanography* **20** (2005).
- [60] Miller, K. G. *et al.* High tide of the warm pliocene: Im-  
plications of global sea level for antarctic deglaciation.  
*Geology* **40**, 407–410 (2012).
- [61] Raymo, M. E., Kozdon, R., Evans, D., Lisiecki, L. & Ford,  
H. L. The accuracy of mid-pliocene  $\delta^{18}O$ -based ice volume  
and sea level reconstructions. *Earth-Science Reviews* **177**,  
291–302 (2018).

- 678 [62] Gasson, E., DeConto, R. M. & Pollard, D. Modeling the  
679 oxygen isotope composition of the antarctic ice sheet and  
680 its significance to pliocene sea level. *Geology* **44**, 827–830  
681 (2016).
- 682 [63] Jansen, E., Fronval, T., Rack, F. & Channell, J. E. T.  
683 Pliocene-pleistocene ice rafting history and cyclicity in  
684 the nordic seas during the last 3.5 myr. *Paleoceanography*  
685 **15**, 709–721 (2000).
- 686 [64] Bierman, P. R., Shakun, J. D., Corbett, L. B., Zimmerman,  
687 S. R. & Rood, D. H. A persistent and dynamic east green-  
688 land ice sheet over the past 7.5 million years. *Nature* **540**,  
689 256–260 (2016).

# SUPPLEMENTARY INFORMATION FOR: AN EARLY PLIOCENE RELATIVE SEA LEVEL RECORD FROM PATAGONIA (ARGENTINA)

PREPRINT, COMPILED JULY 3, 2020

Alessio Rovere<sup>1\*</sup>, Marta Pappalardo<sup>2</sup>, Sebastian Richiano<sup>3</sup>, Marina Aguirre<sup>4</sup>, Michael R. Sandstrom<sup>5</sup>, Paul J. Hearty<sup>6</sup>, Jacqueline Austermann<sup>5</sup>, Ignacio Castellanos<sup>7</sup>, and Maureen E. Raymo<sup>5</sup>

<sup>1</sup>MARUM - Center for Marine Environmental Sciences, University of Bremen

<sup>2</sup>Department of Earth Sciences, Università degli studi di Pisa

<sup>3</sup>Instituto Patagónico de Geología y Paleontología, CONICET, Puerto Madryn

<sup>4</sup>CONICET, CCT-La Plata and Universidad Nacional de La Plata

<sup>5</sup>Lamont Doherty Earth Observatory, Columbia University

<sup>6</sup>Department of Geological Sciences, Jackson School of Geosciences, The University of Texas at Austin

<sup>7</sup>Baker Hughes

## PALEO RELATIVE SEA LEVEL INDICATORS IN PATAGONIA

The study of paleo shorelines in Patagonia dates back to Charles Darwin, who was the first to provide an account of the coastal stratigraphy in the region<sup>1</sup>. Nearly a century later, the Italian geologist Feruglio reported the first full account of marine terraces along the Patagonian coast (Chubut and Santa Cruz Provinces)<sup>2</sup>, that he grouped into six systems. The two uppermost systems attributed to the late Pliocene–early Pleistocene<sup>3</sup> based on biostratigraphic features and their high elevation (40–50 and 80–95 m asl). Several studies detailed the stratigraphy, elevation and age of Holocene<sup>4,5</sup>, Pleistocene<sup>6,7,8,9,10,11,12</sup> and Pliocene–Miocene<sup>13,14</sup> marine and coastal deposits. The Tertiary marine sediments were assigned to Miocene and Pliocene periods mostly on the basis of biostratigraphy. Several authors worked to characterize the Marine Miocene of Patagonia<sup>15,16,17</sup> and the Mio-Pliocene<sup>18</sup>. For which concerns the Early Pliocene, a marine deposit in Northern Patagonia (Rio Negro Province) yielded a fission track age of 4.41 Ma<sup>19</sup>, but this age was later considered inconsistent with biostratigraphic characteristics of the deposits and thus rejected<sup>20</sup>. Del Río et al<sup>14</sup> dated samples of mollusks from marine deposits in Central and Southern Patagonia, few hundreds kilometers south of our study area. The marine deposits of Cerro Laciár (300 km south of the area investigated by this study, 170–185m above MSL) yielded ages of 5.10 ± 0.21 Ma, and those of Cañadon Darwin (540 km south of the area investigated by this study, 65–75m above MSL) yielded ages of 5.15 ± 0.18 Ma. These two data points represent the first geochemically constrained evidence of a (Early) Pliocene transgression in the area.

In the coastal area around the Camarones town, the lithology is characterized by a Jurassic volcanic complex (Complejo Marifil), and Upper Paleocene sedimentary rocks (Formación Río Chico)<sup>21</sup>. According to the official geological charts<sup>21</sup>, the volcanic complex is composed by reddish rhyolites, leucorhyolites and ignimbrites, whereas the Río Chico formation is made of mudstones, sandstones and conglomerates, often volcanoclastic. Along the same coastal section, fossil beach ridges and marine/beach deposits were recognized from present-day coastline inland.

**Holocene.** Holocene sea level indicators have been preserved at Camarones as series of proxies marking the maximum sea level transgression and a sequence of regressive beach ridges.

Bini et al., 2018<sup>22</sup> reported precisely measured Holocene RSL proxies dated with <sup>14</sup>C, indicating that, between ca. 5300 and 7000 cal. yr BP, RSL was 2 to 4 m above present sea level (elevations referred to the EGM2008 Geoid).

**Marine Isotopic Stage 5e.** The Last Interglacial is also preserved in the form of relic beach ridges in the Camarones area. These were studied by different authors throughout the years<sup>9,12,10,23</sup>, and were dated to MIS 5e using Electron Spin Resonance and U-Series on mollusks (Supplementary Table 1). A recent study by Pappalardo et al. 2015<sup>9</sup> provides more precise measurements, interpretations and additional dating of the MIS 5e beach ridge complex at Camarones. According to these authors, the MIS 5e beach ridges at Camarones were formed in correspondance with a paleo RSL at 7.5 +2/-3.5m above present.

**Marine Isotopic Stage 11.** At one site south of Camarones town, articulated shells from (Sample Pa 35) was dated by Schellmann and Radtke (2000)<sup>12</sup> as MIS 9 or older. U-series mollusk ages by Pappalardo et al. (2015)<sup>9</sup> confirm the attribution to MIS 11. We measured the deposits dated by these authors at 16.7 ± 0.4m above present sea level.

## DETAILED DESCRIPTION OF *Roadcut* AND *Caprock* UNITS AT CAMARONES

The *Roadcut* section (Supplementary Figure 1) is characterized by the bedrock (Río Chico formation) outcropping from the road level up to ca.12m above it, mostly sheltered by a tick debris. The topmost part of the bedrock is exposed for a maximum thickness of 1.2m in the western part of the outcrop and it is shaped as a flat, gently eastward (i.e. seaward) dipping platform. All the overlying units are separated from it by a sharp erosional unconformity. Less than 1 km south of the *Roadcut*, another outcrop shows the same geological context. We refer to this as the *Caprock* outcrop (Supplementary Figure 2). This rests on a relative topographic high of the bedrock, which in this point is represented by the volcanic Complejo Marifil, capped by a thin sedimentary unit, as thick as 1m maximum, identical to the upper part of the Cp Unit observed in the *Roadcut* section. Each overlying unit is described separately hereafter.

Table S 1: Ages of beach ridges associated to MIS 5e in the Camarones area.

Location	Author	Sample	Subsample	Age (ka)	Age uncertainty (ka)	Dating technique	
Camarones North IV	Schellmann (1998) <sup>23</sup>	Pa 30	D2412A	117	21	ESR	
			D2635	123	22	ESR	
			K2412B	139	8	ESR	
			D2550	92	9	ESR	
			D2549	99	12	ESR	
Camarones North I	Schellmann (1998) <sup>23</sup>	Pa 47c	D2665	115	9	ESR	
			D2547	117	13	ESR	
			D2546	133	15	ESR	
			D2545	137	18	ESR	
			D2548	144	19	ESR	
Camarones 12km South	Rostami et al., 2000 <sup>10</sup>	3	3-0/1	117	5	U-Series	
			3-0/2	115	9	U-Series	
			3-0/2	110	8	ESR	
			3-0/3	112	13	U-Series	
			3-0/3	114	9	ESR	
			WP64A(3)	N/A	121	0.9	U-Series
			WP65(1)	N/A	130	2.5	U-Series
Various sites North and south of Camarones	Pappalardo et al., 2015 <sup>9</sup>	WP68(1)	N/A	131	1.1	U-Series	
			WP70(B)	N/A	127	1.2	U-Series

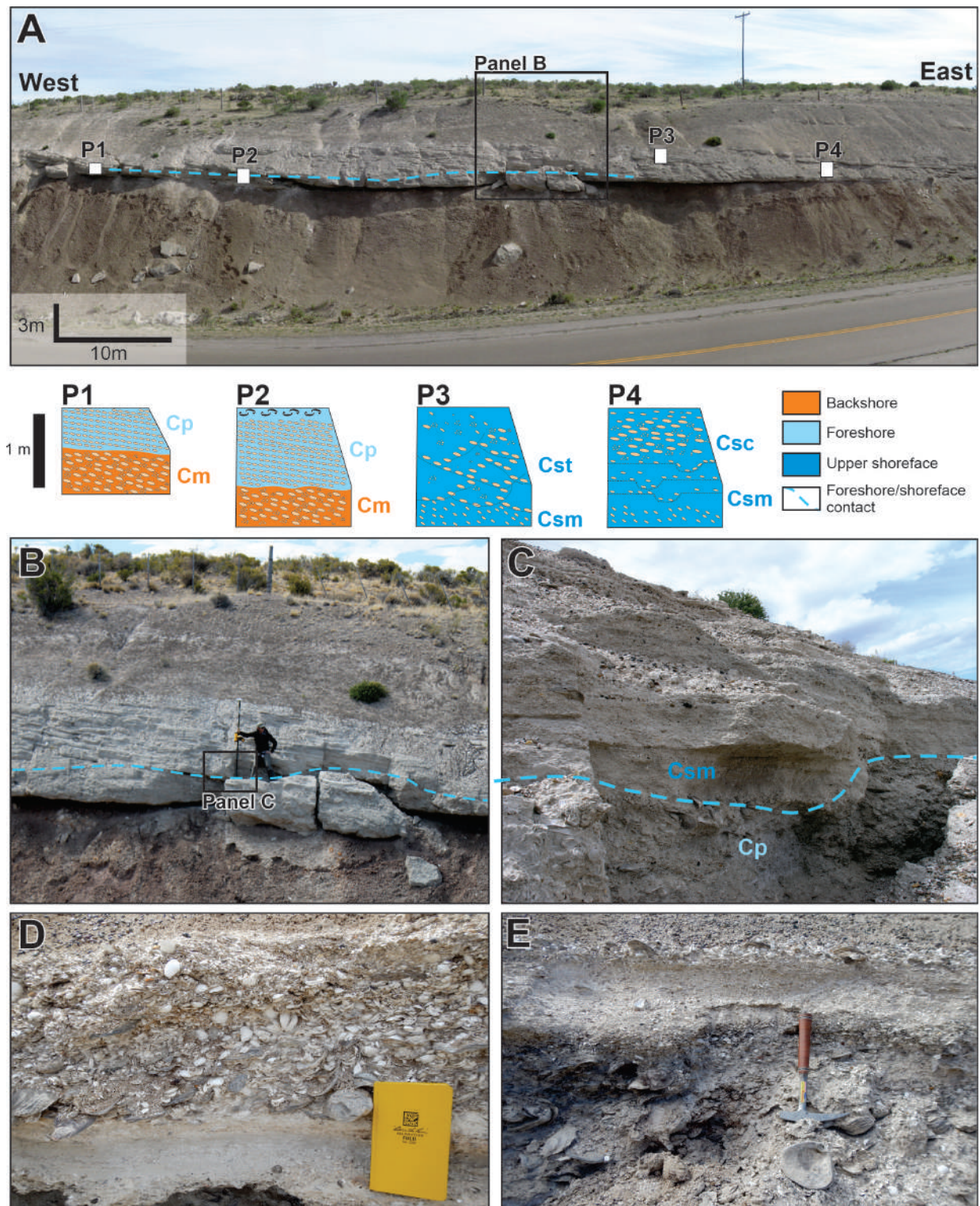
80 **Unit Cm.** In the western part of the section on top of the  
81 bedrock rests a basal unit (Cm). This is represented by a mas-  
82 sive, clast-supported conglomerate with coarse rounded pebbles  
83 of different rock types. Pebbles have an imbricated, seaward  
84 dipping bedding. Faunal content is absent.

85 **Unit Cp.** Eastward, a finer unit (Cp) overlaps the previous  
86 one and, towards the East, unconformably rests on the bedrock.  
87 Unit Cp is composed of well-cemented fine conglomerates with  
88 rounded pebbles, mostly unbroken shells and abundant sandy  
89 matrix, displaying a low-angle planar cross-stratification. The  
90 uppermost part of Cp contains a dense faunal assemblage in  
91 the form of a shellbed, with different shell types (Supplemen-  
92 tary Table 2) mostly intact and sometimes with paired valves  
93 (articulated), but not in living position. Only the fragmentation  
94 of Pectinids is relevant, which is expected even with scarce  
95 transport as they have a fragile shell structure. The shells in  
96 Unit Cp are characterized by different stages of preservation, de-  
97 pending mostly on the shell type. Big oysters (*Crassostrea* sp.),  
98 up to 15 cm in size, are frequent, mostly oriented concordant  
99 with strata dip and strike. They underwent partial dissolution,  
100 especially of their outer part, which explains the high degree  
101 of cementation of this unit. The faunal assemblage of Unit  
102 Cp is analogous to that of the Pleistocene terraces towards the  
103 coast, with notable exceptions. The absence of *Tegula atra* (cold  
104 gastropod species), together with the occurrence of bivalves of  
105 warm/warm-temperate affinity (*C. patagonica*, *D. patagonica*, *F.*  
106 *vilardebona*, *M. cf. isabelleana*), is the main difference relative  
107 to the Pleistocene deposits. Cp has a maximum thickness of  
108 1m in the western part of the outcrop (stratigraphic column B,  
109 Supplementary Figure 1B).

110 **Unit Cs.** East of this point, the Cp unit becomes progres-  
111 sively thinner, and is overlapped by a finer unit (Cs) of matrix-  
112 supported sandy conglomerates. The contact between Cp and  
113 Cs is planar and displays a lateral continuity up to the midpoint  
114 of the section, East of which Cs lays directly on the bedrock.  
115 The basal part of Cs is massive (Csm) with no sedimentary  
116 structures, whereas its uppermost part, separated from Csm by

a gradational contact, displays trough cross-stratification (Cst) and, more eastward, longitudinal channels (Csc).

Overall, this section represents the product of sedimentation due to a transgressive event on top of a marine platform carved in the volcanic bedrock. The sequence is fining (and thus deepening) upward. The similarities of the basal unit (Cm) with modern storm berms in the area suggest that it was formed in a backshore environment. We interpret Unit Cp as the product of sedimentation in a foreshore environment. The bedding of marine shells within this unit testifies that they have been re-handled within the surf zone where sediments from upper offshore and shoreface are floated towards the beachface and from there are driven back by rip currents, producing an isorientation of single shells parallel to the current direction. The topmost Units (Csm, Cst and Csc) can be interpreted as mainly developed in middle to upper shoreface. The sedimentary structures within these units can be interpreted as the product of longitudinal currents caused by coastal drift.



Supplementary Figure 1: A) General view of the *Roadcut* section. Below the photo, four stratigraphic profiles (P1-P4) detailing the relationships between the main sedimentary facies. **Cm**: Conglomerate, massive; **Cp**: Conglomerate with low angle planar cross-stratification; **Csm**: Sandy conglomerate, massive; **Cst**: Sandy conglomerate with trough cross-stratification; **Csc**: Sandy conglomerate with longitudinal channels. B) Location where the elevation of unit **Cp** has been measured (the points listed in the main paper are located near the person standing on the outcrop). C) Detail of the contact between **Cp** (foreshore) and **Csm** (upper foreshore). D) and E) Details of the bivalve-rich horizon sampled for Sr isotopes dating.

Table S 2: Faunal assemblage in the marine deposits outcropping at the *Roadcut* section at Camarones. Most of the species recognized by Feruglio<sup>3,2</sup> and assigned to the highest terrace system (that was tentatively dated to Pliocene) were detected in the Cp Unit of the *Roadcut* section (This work). Nomenclature of the taxa has been updated as some generic or specific names do not agree with those used by Feruglio. \* indicates species with warm/warm-temperate affinity.

BIVALVIA	Feruglio works	This work
<i>Aulacomya atra</i> (Molina, 1782)	X	X
<i>Aequipecten tehuelchus</i> (d'Orbigny, 1842)	X	
<i>Zygochlamys patagonica</i> (King, 1832)	X	X
<i>Pectinidae indet.</i>		X
<i>Ostrea equestris</i> Say, 1834		X
<i>Ostrea puelchana</i> d'Orbigny, 1842	X	
<i>Ostrea tehuelcha</i> Feruglio	X	X
<i>Ostrea cf. tehuelcha</i> Feruglio		X
<i>Ostrea sp</i>		X
<i>Ostrea tehuelcha</i> d'Orbigny*		X
<i>Diplodonta patagonica</i> (d'Orbigny, 1842)*		X
<i>Felaniella vilardeboana</i> (d'Orbigny, 1846)*	X	
<i>Diplodonta sp</i>	X	
<i>Abra sp</i>		X
<i>Mactra cf. isabellena</i> d'Orbigny, 1846*	X	X
<i>Mactra cf. patagonica</i> d'Orbigny		X
<i>Eurhomalea exalbida</i> (Dilwyn, 1817)		
<i>Ameghinomya antiqua</i> (King, 1832)		X
<i>Pitar rostratus</i> (Philippi, 1844)	X	X
<i>Corbula patagonica</i> d'Orbigny 1845	X	X
<b>GASTROPODA</b>		
<i>Epitonium georgettinum</i> (Kiener, 1838)	X	X
<i>Trophon varians</i> (d'Orbigny, 1841)	X	X
<i>Trophon geversianus</i> (Pallas, 1774)	X	X
<i>Trophon laciniatus</i> (Martin)	X	X
<i>Adelomelon ancilla</i> (Lightfoot, 1786)	X	X
<i>Adelomelon ferussaci</i> (Donovan, 1824)		
<i>Adelomelon sp</i>		X
<i>Odontocymbiola magellanica</i> (Gmelin, 1791)	X	X
<i>Olivancillaria auricularia</i> (Lamarck, 1811)	X	X
<i>Olivancillaria cf. carcellesi</i> Klappenbach, 1965		
<i>Buccinanops deformis</i> (P.P. King, 1832)	X	X
<i>Buccinanops cochlidium</i> (Dilwyn, 1817)	X	
<i>Buccinanops sp</i>	X	X
<i>Siphonaria lessonii</i> Blainville, 1827		
<i>Volutidae indet.</i>	X	X

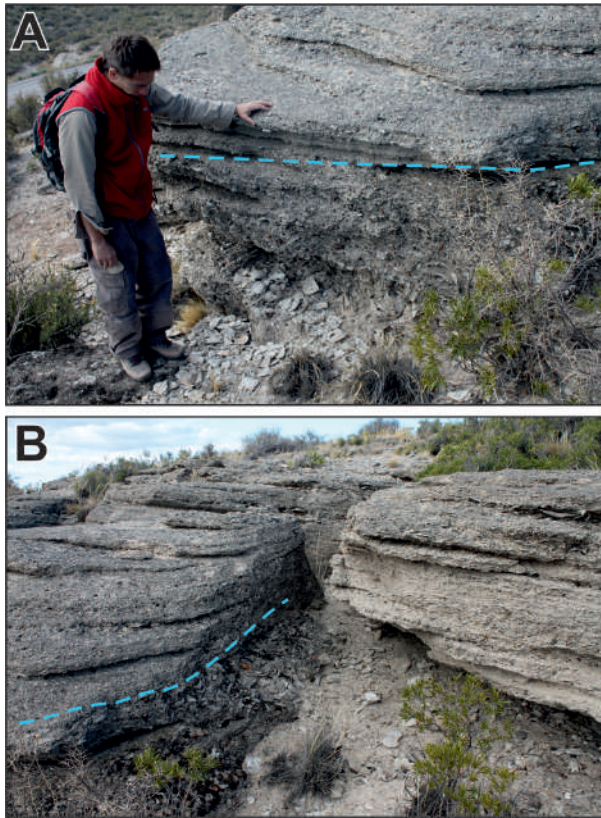
### 135 SUPPLEMENTARY AGE INFORMATION.

136 Details on samples and SIS analyses performed are shown here-  
137 after, in Supplementary Figures 3 to 7. Full SIS age results are  
138 reported in Supplementary Table 4.

139 Initial field selection criteria involved visual assessment based on  
140 shell thickness, coloration, and diagnostic features of preserva-  
141 tion, including microborings, Fe and Mg staining, fragmentation  
142 of original layers, and irregularities in structure<sup>14,24,25</sup> (Supple-  
143 mentary Figure 4). In the laboratory, samples were slabbed,  
144 polished and imaged using an optical microscope with CCD  
145 camera for further inspection, and an ASPEX Express scanning  
146 electron microscope (SEM). This preliminary screening method  
147 helps identify locations of alteration that can be correlated with  
148 the <sup>87</sup>Sr/<sup>86</sup>Sr leach variations and establishes the overall integrity

of preservation in each shell. A preservation scoring system was  
149 established as outlined in Hearty et al. (2020)<sup>26</sup>, with optical  
150 and SEM images assigned scores from "1" (no visible alteration)  
151 to "3" (significant alteration observable) based on screening  
152 criteria above (Supplementary Table 3).  
153

154 Shells were micro sampled in the best-preserved regions and  
155 homogenized into a fine powder using a dremel drill or acid-  
156 cleaned agate mortar and pestle (except for sample ACC1-A pt2,  
157 which was kept as a fragment for Sr isotope analysis). Minor and  
158 trace elements were measured for three samples on a Thermo  
159 iCap Q quadrupole ICP-MS at LDEO. Samples were prepared  
160 and analyzed following methods similar to Yu et al<sup>27</sup>. Briefly,  
161 ca.250 µg of powder was diluted to 75 ppm Ca (to negate matrix  
162 effects), and run alongside calibration standards covering the



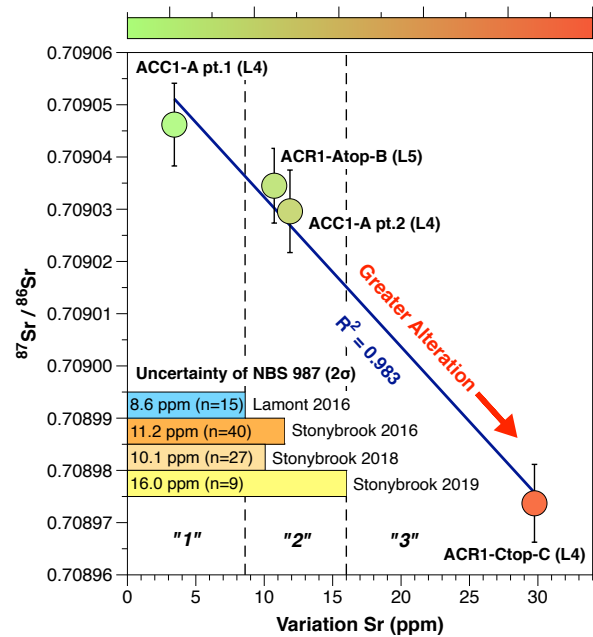
Supplementary Figure 2: A) and B) Contact between the unit Cp (lower) and Cs (higher) at the Caprock site.

163 range of elements concentrations. The results were normalized  
 164 to the in-house reference standards QC-Calcite and planktonic  
 165 standard V03, the latter of which has long-term ( $n = 86$ )  $2\sigma$   
 166 errors of: Sr/Ca = 1.4%, Mg/Ca = 1.3%, U/Ca = 3.0%, Ba/Ca  
 167 = 1.8%, Mn/Ca = 1.2%, Al/Ca = 15.8%, Fe/Ca = 2.1% and  
 168 Na/Ca = 1.3%. A Holocene bivalve (*Tridactna gigas* standard  
 169 JCT-1) was run alongside the samples for comparison. An el-  
 170 emental scoring system was established for Mg, Mn, and Fe  
 171 (Supplementary Table 3), elements thought to be indicative of  
 172 diagenesis<sup>28;29;26</sup>. Scores ranged from "1" (unaltered) to "3"  
 173 (altered) based on comparison to a set of Holocene corals and  
 174 bivalves (see Sandstrom et al., in review). Sample splits were  
 175 taken for Sr isotope analysis (ca. 50 mg for leach fraction, and  
 176 ca. 10 mg for full dissolution).

177 Leaching procedures are modified from Bailey et al<sup>30</sup> (see  
 178 Hearty et al., 2020<sup>26</sup>), and involve weak (ca. 0.1M) Acetic  
 179 acid leaches on the powdered/fragmented shell, designed to pre-  
 180 ferentially dissolve the more loosely bound secondary  $^{87}\text{Sr}/^{86}\text{Sr}$   
 181 material before attacking the primary Sr. Typically, four to five  
 182 leaches were performed per sample, each dissolving ca. 12mg  
 183 (20-25%) of the material, along with one full dissolution of a  
 184 separate split to average the bulk  $^{87}\text{Sr}/^{86}\text{Sr}$  ratio. Only the initial  
 185 and inner leaches were measured, along with full dissolution  
 186 splits (Supplementary Table 4 and Supplementary Figure 5). Sr  
 187 was isolated and dried down using typical separation techniques  
 188 with Eichon exchange resin. Following separation, 1% of Sr  
 189 was removed and measured on a mass spectrometer to determine  
 190 concentration. A drop of 0.05 N Phosphoric acid was added

and 150-375 ng Sr was loaded onto degassed Rhenium filaments  
 using tantalum chloride loader.

191  
 192

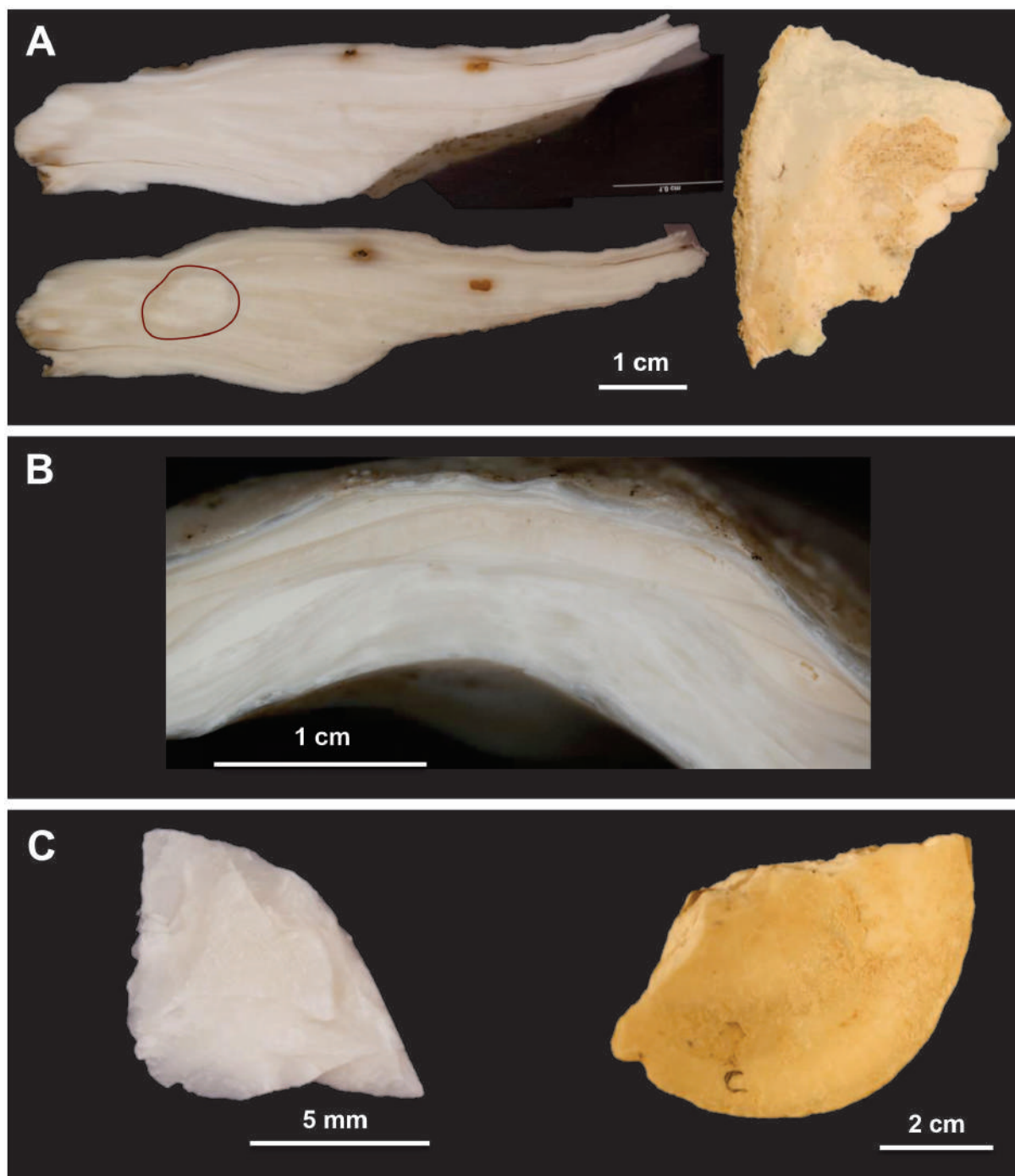


Supplementary Figure 3: Variation of  $^{87}\text{Sr}/^{86}\text{Sr}$  within a leach set (as ppm) vs. the inner leach  $^{87}\text{Sr}/^{86}\text{Sr}$  of that shell. Sr leach variation scores are shown by dashed black line; these scores are based on the range of ppm error from seasonal long-term averages of the standard NBS 987. Green circles have low variation within leach sets (usually better preservation) and display younger SIS ages than shell ACC1-Ctop-C (red point) with high variation. This sample is excluded from the average shoreline SIS age based on high Sr variation and other screening criteria (Supplementary Table 3). Long-term uncertainty of standard NBS987 for each year/lab plotted on lower left as ppm variation.

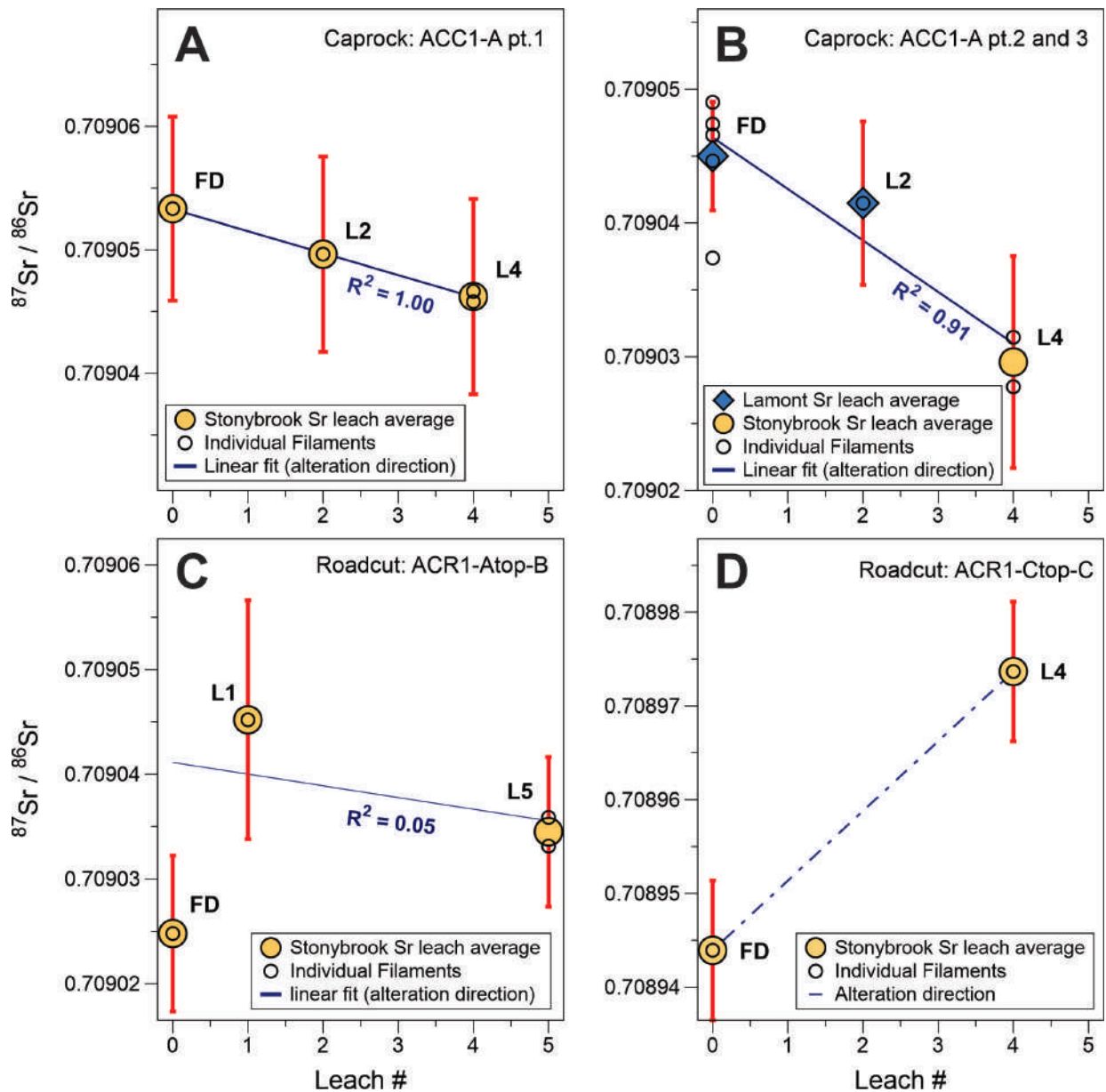
193  $^{87}\text{Sr}/^{86}\text{Sr}$  ratios were measured on either an IsotopX Phoenix62  
 194 Thermal Ionization Mass Spectrometer (TIMS) at Stonybrook  
 195 University, or a Finnigan Triton Plus TIMS at Lamont-Doherty  
 196 Earth Observatory (LDEO). Measurements at Stonybrook were  
 197 conducted in a very similar manner to Gothmann et al<sup>29</sup>, with a  
 198 dynamic routine measuring masses 84, 85, 86, 87, and 88 over  
 199 160 cycles for each sample. Filaments were slowly ramped up  
 200 to 2.8 - 3.2 A and a temperature of ca. 1400 degrees Celsius,  
 201 to achieve a beam intensity between 3-5 V on mass 88. TIMS  
 202 measurements at LDEO were carried out using a static rou-  
 203 tine for 200-400 cycles with similar parameters to Stonybrook.  
 204 The Sr isotope external standard NBS SRM 987 long-term in-  
 205 strument accuracy at the two labs was computed every season  
 206 and ranged between 8.6 - 16 ppm ( $2\sigma$ ) (Supplementary Figure  
 207 3). At Stonybrook: NBS 987 =  $0.7102445 \pm 0.0000079$  ( $2\sigma$ ;  
 208 2016,  $n = 40$ );  $0.7092414 \pm 0.0000072$  ( $2\sigma$ ; 2018,  $n = 27$ ), and  
 209  $0.7102437 \pm 0.0000114$  ( $2\sigma$ ; 2019,  $n = 9$ ) and at LDEO: NBS  
 210 987 =  $0.7102375 \pm 0.0000061$  ( $2\sigma$ ; 2016,  $n = 15$ ). Sr isotopes  
 211 were all corrected for mass fractionation based on an  $^{86}\text{Sr}/^{88}\text{Sr}$  Sr  
 212 ratio of 0.1194 and normalized to the accepted NBS 987 standard  
 213 value = 0.709248. Sr isotope stratigraphy ages were calculated  
 214 using the LOWESS version 5 curve from McArthur et al<sup>28</sup>. Sr



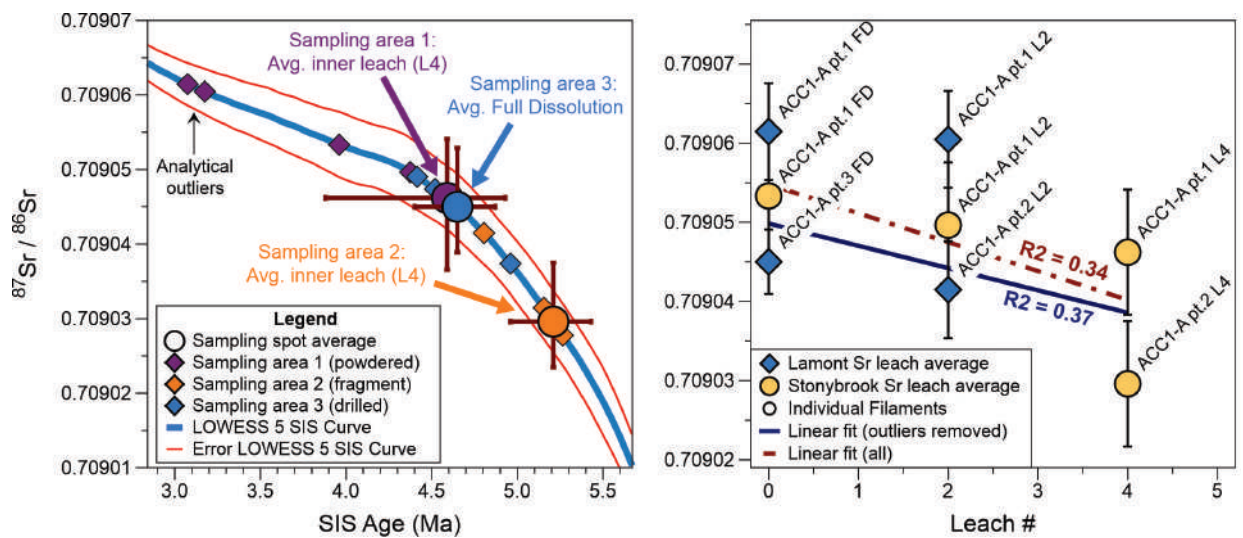
215 isotope variations (in ppm) within leach sets were calculated for  
216 each sample (Supplementary Table 3) and a scoring system from  
217 "1" to "3" was established based on long-term uncertainties of  
218 NBS 987 (see figure S3 and Sandstrom et al., in review).



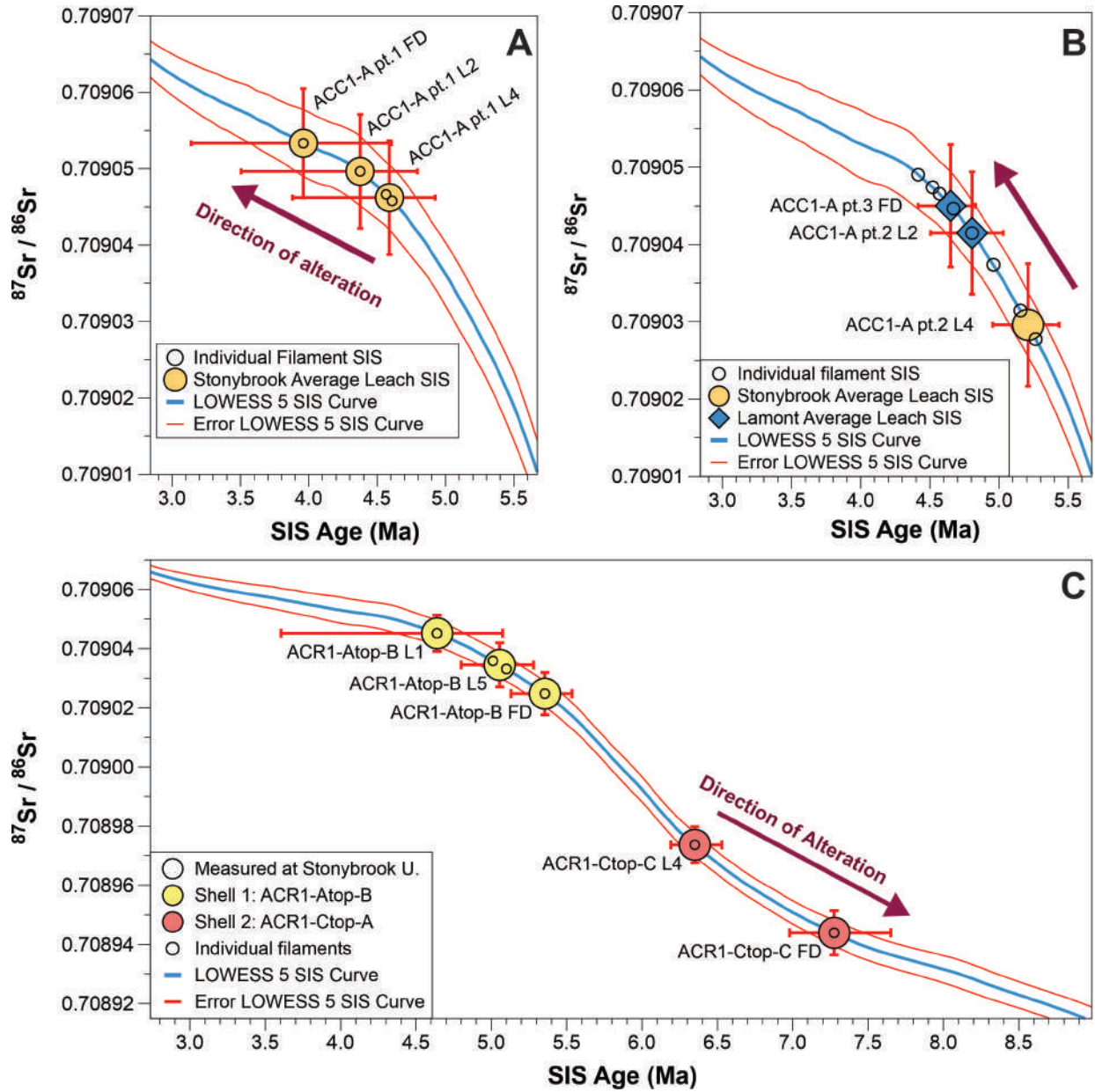
Supplementary Figure 4: Sample images. A) Oyster shell ACC1-A, showing slabbed x-section (top left), part 3 drill location (bottom left), and original shell fragment (right). B) Sample ACR1-Atop-B slabbed x-section. C) Shell ACR1-Ctop-C showing fragment used in Sr isotope dating (left) and partial shell collected from the field (right).



Supplementary Figure 5: Sr isotope leach set data for individual sample areas. Red error bars represent  $2\sigma$  external uncertainty of NBS987 (except for full dissolution ACC1-A pt.3 FD, which is  $2\sigma$  standard error of the mean). Linear regression lines (blue) indicate direction of alteration, with altering fluids causing the *Caprock* oyster (A and B) to appear slightly younger (more radiogenic  $^{87}\text{Sr}/^{86}\text{Sr}$ ), and the *Roadcut* samples (C and D) to appear older (alteration fluid with low  $^{87}\text{Sr}/^{86}\text{Sr}$ ). A and B) Leach set data for sample ACC1-A parts 1 and 2 showing less radioactive  $^{87}\text{Sr}/^{86}\text{Sr}$  (increased SIS age) with better preservation (L4). C) The inner leach lies between the initial leach and full dissolution, overlapping both within uncertainty. The leach set suggests alteration fluids cause ages to appear younger, while the full dissolution indicates the opposite. However, based upon the excellent preservation index score, the inner leach (L5) most likely reflects the original Sr isotopic ratio. D) The trend of significantly increasing  $^{87}\text{Sr}/^{86}\text{Sr}$  of the inner leach compared to the full dissolution indicates post-depositional alteration in this sample.



Supplementary Figure 6: Oyster shell ACC1-A (*Caprock*) detailed Sr isotopes and SIS age assignments from three different sampling locations (Left panel). Right panel shows leach Sr values and different TIMS machines (yellow = stonybrook, blue = Lamont). Sample splits ACC-1A pt.1 FD and L2 measured at LDEO appear to be outliers for reasons unknown [possibly turret related? as this was the first turret run?]. Repeated measurements on these same splits at SBU yielded more reliable  $^{87}\text{Sr}/^{86}\text{Sr}$  values that more closely align with other measurements from different sections of this shell, both at SBU and LDEO. Linear regression was computed for all leach averages (red) and also excluding the two outliers (blue) with similar results. There is a slight trend toward less radiogenic values for the better preserved inner leach measurements.



Supplementary Figure 7: Same data as Supplementary Figure 5. Sr isotope leach set data for individual sample areas, plotted against Lowess5 SIS curve. Red error bars represent  $2\sigma$  external uncertainty of NBS987 (except for full dissolution ACC1-A pt.3 FD, which is  $2\sigma$  standard error of the mean). Purple arrows indicate direction of alteration, with altering fluids causing the *Caprock* oyster (A and B) to appear younger (more radioactive  $^{87}\text{Sr}/^{86}\text{Sr}$ ), and the *Roadcut* samples (C) to appear older (in the case of ACR1-Ctop-C), and possibly younger in the case of ACR1-Atop-A, but no distinct trend can be assigned.

Table S 3: Elemental and diagenetic screening results of oyster samples. BDL = below detection limit. n.a. = not measured. <sup>a</sup> Jct-1 is the Holocene Tridactna standard<sup>31</sup>. <sup>b</sup> Samples used in elemental score average. <sup>c</sup> Full dissolution used for variation calculation, as L1 was not measured. <sup>d</sup> Scoring criteria outlined in Sandstrom et al., in review. <sup>e</sup> See Supp. methods and Hearty et al. (2020)<sup>26</sup>. <sup>f</sup> Leach variation scores: "1" = <8.6ppm; "2" = 8.6 to 16 ppm; "3" = >16 ppm. <sup>g</sup> Samples with preservation index scores  $\geq$  "2" are considered altered and excluded.

Sample Code	ACC1-A pt.1	ACR1-Atop-B	ACR1-Ctop-C	Jct-1 <sup>a</sup>
SEsar ISGN ID	Requested	Requested	Requested	N/A
Description	Caprock - Oyster	Roadcut - Oyster	Roadcut - Oyster	Holocene Tridactna
Na/Ca (mmol/mol)	8.1	9.5	11.7	19.9
Mg/Ca (mmol/mol) <sup>b</sup>	2.9	3.3	4.9	1.2
Al/Ca ( $\mu$ mol/mol)	4.6	BDL	20.4	17.2
Mn/Ca ( $\mu$ mol/mol) <sup>b</sup>	78.8	16.2	1484.7	2.6
Fe/Ca ( $\mu$ mol/mol) <sup>b</sup>	1.7	BDL	144.5	BDL
Sr/Ca (mmol/mol)	0.58	0.85	1.50	1.84
Ba/Ca ( $\mu$ mol/mol)	2.2	2.2	5.9	1.6
U/Ca (nmol/mol)	89.2	107.5	155.2	33.3
number of splits	1	2	1	3
<sup>87</sup> Sr/ <sup>86</sup> Sr leach variation (ppm)	11.88	10.73	29.75 <sup>c</sup>	n.a.
Elemental score (1-3) <sup>d</sup>	1.67	1.67	2.33	1.00
SEM score (1-3) <sup>e</sup>	2	n.d.	2	n.a.
Optical score (1-3) <sup>e</sup>	2	1	2	1
<sup>87</sup> Sr/ <sup>87</sup> Sr variation score (1-3) <sup>f</sup>	2	2	3	n.a.
<b>Preservation Index Score<sup>g</sup> (average of all scores: 1-3)</b>	<b>1.92</b>	<b>1.56</b>	<b>2.33</b>	<b>1.00</b>

Table S 4:  $^{87}\text{Sr}/^{86}\text{Sr}$  results and Sr isotope stratigraphy ages for Caprock and Roadcut outcrops. <sup>a</sup> Inner leach Sr isotope values for sample; <sup>b</sup> Sample leaches excluded based on analytical or diagenetic criteria; <sup>c</sup> Sample excluded from shoreline age based on significant diagenesis (see Table S3); <sup>d</sup> Uncertainty based on  $2\sigma$ SEM; <sup>e</sup> Sample variation is calculated as the difference between the initial leach [or full dissolution] and last leach, multiplied by one million (ppm); <sup>f</sup> Average of inner leaches on samples that passed screening criteria: ACC1-A pts. 1 and 2, and ACRI-Atop-B; <sup>g</sup> Uncertainty based on combined analytical [ $2\sigma$ SEM] and SIS curve [LOWESS 5] errors.

Sample Name	TIMS Lab	Leach ID	Nb. filaments	$^{87}\text{Sr}/^{86}\text{Sr}$ (measured)	$^{87}\text{Sr}/^{86}\text{Sr}$ (normalized to NBS97)	$2\sigma$ external uncertainty	Mean SIS Age (Ma)	Maximum SIS Age (Ma)	Minimum SIS Age (Ma)	Uncorrected SIS Age (Ma)
<b>Average <math>^{87}\text{Sr}/^{86}\text{Sr}</math> by Leach</b>										
<b>Caprock</b>										
ACC1-A pt.1 FD	SBU	FD	1	0.7090465	0.7090533	0.0000075	3.960	4.605	3.140	4.58
ACC1-A pt.1 L2	SBU	L2	1	0.7090462	0.7090496	0.0000079	4.375	4.795	3.505	4.59
ACC1-A pt.1 L4 <sup>a</sup>	SBU	L4	2	0.7090427	0.7090462	0.0000079	4.590	4.925	3.880	4.76
ACC1-A pt.1 FD <sup>b</sup>	LDEO	FD	1	0.7090509	0.7090615	0.0000061	3.075	3.745	2.635	4.27
ACC1-A pt.1 L2 <sup>b</sup>	LDEO	L2	1	0.7090499	0.7090605	0.0000061	3.175	3.855	2.695	4.36
ACC1-A pt.2 L2	LDEO	L2	1	0.7090309	0.7090415	0.0000061	4.805	5.030	4.505	5.17
ACC1-A pt.2 L4 <sup>a</sup>	SBU	L4	2	0.7090261	0.7090296	0.0000079	5.210	5.435	4.955	5.32
ACC1-A pt.3 FD	LDEO	FD	5	0.7090345	0.7090344	0.0000041 <sup>d</sup>	4.650	4.415	4.830	5.055
<b>Roadcut</b>										
ACRI-Atop-B FD	SBU	FD	1	0.7090180	0.7090248	0.0000075	5.355	5.535	5.130	5.52
ACRI-Atop-B L1	SBU	L1	1	0.7090409	0.7090452	0.0000114	4.640	5.075	3.605	4.83
ACRI-Atop-B L5 <sup>a</sup>	SBU	L5	2	0.7090279	0.7090345	0.0000072	5.055	5.280	4.800	5.27
ACRI-Ctop-C FD	SBU	FD	1	0.7089371	0.7089439	0.0000075	7.275	7.650	6.980	7.62
ACRI-Ctop-C L4 <sup>a,c</sup>	SBU	L4	1	0.7089668	0.7089737	0.0000075	6.350	6.530	6.190	6.52
<b>Average Shoreline SIS Age</b>										
Average of screened inner leaches <sup>f</sup>	SBU	L4, L5	6	0.7090322	0.7090368	0.0000064 <sup>d</sup>	4.98	5.225 <sup>g</sup>	4.685 <sup>g</sup>	5.13

## 219 REFERENCES

- 220 [1] Darwin, C. *Geological observations on South America: Being the third part of the geology of the voyage of the*  
 221 *Beagle, under the command of Capt. Fitzroy, RN during*  
 222 *the years 1832 to 1836* (Smith, Elder and Company, 65,  
 223 Cornhill., 1846).  
 224
- 225 [2] Feruglio, E. *I terrazzi marini della Patagonia* (Cooperativa  
 226 Tip. Edit. Paolo Galeati, 1933).
- 227 [3] Feruglio, E. *Descripción geológica de la Patagonia*, vol. 1  
 228 (Impr. y Casa Editora "Coni", 1949).
- 229 [4] Schellmann, G. & Radtke, U. Coastal terraces and  
 230 holocene sea-level changes along the patagonian atlantic  
 231 coast. *Journal of Coastal Research* 983–996 (2003).
- 232 [5] Zanchetta, G. *et al.* Middle-to late-holocene relative sea-  
 233 level changes at puerto deseado (patagonia, argentina). *The*  
 234 *Holocene* **24**, 307–317 (2014).
- 235 [6] Bini, M. *et al.* Markers of palaeo sea-level in rocky coasts  
 236 of patagonia (argentina). *Rendiconti Online della Società*  
 237 *Geologica Italiana* **20**, 10–14 (2013).
- 238 [7] Fucks, E. *et al.* Influence of quaternary sea level changes in  
 239 the littoral of chubut, argentina. *Journal of South American*  
 240 *Earth Sciences* **88**, 589–598 (2018).
- 241 [8] Pappalardo, M. *et al.* Challenges in relative sea-level  
 242 change assessment highlighted through a case study: The  
 243 central coast of atlantic patagonia. *Global and Planetary*  
 244 *Change* **182**, 103008 (2019).
- 245 [9] Pappalardo, M. *et al.* Coastal landscape evolution and  
 246 sea-level change: A case study from central patagonia  
 247 (argentina). *Zeitschrift für Geomorphologie* **59**, 145–172  
 248 (2015).
- 249 [10] Rostami, K., Peltier, W. & Mangini, A. Quaternary marine  
 250 terraces, sea-level changes and uplift history of patago-  
 251 nia, argentina: comparisons with predictions of the ice-4g  
 252 (vm2) model of the global process of glacial isostatic ad-  
 253 justment. *Quaternary Science Reviews* **19**, 1495–1525  
 254 (2000).
- 255 [11] Pedoja, K. *et al.* Uplift of quaternary shorelines in eastern  
 256 patagonia: Darwin revisited. *Geomorphology* **127**, 121–  
 257 142 (2011).
- 258 [12] Schellmann, G. & Radtke, U. ESR dating stratigraphically  
 259 well-constrained marine terraces along the patagonian at-  
 260 lantic coast (argentina). *Quaternary International* **68**, 261–  
 261 273 (2000).
- 262 [13] Rutter, N. *et al.* Correlation and dating of quaternary  
 263 littoral zones along the patagonian coast, argentina. *Qua-*  
 264 *ternary Science Reviews* **8**, 213–234 (1989).
- 265 [14] Del Río, C., Griffin, M., McArthur, J., Martínez, S. &  
 266 Thirlwall, M. Evidence for early pliocene and late miocene  
 267 transgressions in southern patagonia (argentina): 87sr/86sr  
 268 ages of the pectinid "chlamys" actinodes (sowerby). *Jour-*  
 269 *nal of South American Earth Sciences* **47** (2013).
- 270 [15] del Río, C. J., Martínez, S. A. & Scasso, R. A. Nature  
 271 and origin of spectacular marine miocene shell beds of  
 272 northeastern patagonia (argentina): Paleoecological and  
 273 bathymetric significance. *Palaios* **16**, 3–25 (2001).
- [16] Dozo, M. T. *et al.* Late miocene continental biota in north-  
 274 eastern patagonia (península valdés, chubut, argentina).  
 275 *Palaeogeography, Palaeoclimatology, Palaeoecology* **297**,  
 276 100–109 (2010).  
 277
- [17] Farinati, E. & Zavala, C. Trace fossils on shelly substrate.  
 278 an example from the miocene of patagonia, argentina. *Acta*  
 279 *Geologica Hispanica* **37**, 29–36 (2002).  
 280
- [18] del Río, C. J. Tertiary marine molluscan assemblages of  
 281 eastern patagonia (argentina): a biostratigraphic analysis.  
 282 *Journal of Paleontology* **78**, 1097–1122 (2004).  
 283
- [19] Bigazzi, G., Bonadonna, F., Leone, G. & Zanchetta, G.  
 284 Primeros datos geoquímicos y geocronológicos a partir  
 285 de algunas cineritas del area bonarense (1995).  
 286
- [20] Farinati, E. A. & Zavala, C. A. Asociaciones de  
 287 megafósiles de invertebrados en el neógeno atlántico de la  
 288 patagonia argentina (2005).  
 289
- [21] Lema, H. A. *et al.* Hoja geológica 4566-ii y iv camarones  
 290 (2001).  
 291
- [22] Bini, M. *et al.* Mid-holocene relative sea-level changes  
 292 along atlantic patagonia: new data from camarones, chubut,  
 293 argentina. *The Holocene* **28**, 56–64 (2018).  
 294
- [23] Schellmann, G. *Jungkänozoische Landschaftsgeschichte*  
 295 *Patagoniens (Argentinien): andine Vorlandvergletscherun-*  
 296 *gen, Talentwicklung und marine Terrassen* (1. Auflage,  
 297 Essen: Klartext, 1998, 1998).  
 298
- [24] McArthur, J. M. Recent trends in strontium isotope stratig-  
 299 raphy. *Terra nova* **6**, 331–358 (1994).  
 300
- [25] Cochran, J. K. *et al.* Effect of diagenesis on the sr, o, and  
 301 c isotope composition of late cretaceous mollusks from  
 302 the western interior seaway of north america. *American*  
 303 *Journal of Science* **310**, 69–88 (2010).  
 304
- [26] Hearty, P. J. *et al.* Pliocene-pleistocene stratigraphy and  
 305 sea-level estimates, republic of south africa with implica-  
 306 tions for a 400 ppmv co2 world. *Paleoceanography and*  
 307 *Paleoclimatology* **n/a**, n/a (2020).  
 308
- [27] Yu, J., Day, J., Greaves, M. & Elderfield, H. Determina-  
 309 tion of multiple element/calcium ratios in foraminiferal  
 310 calcite by quadrupole icp-ms. *Geochemistry, Geophysics,*  
 311 *Geosystems* **6** (2005).  
 312
- [28] McArthur, J., Howarth, R. & Shields, G. Strontium isotope  
 313 stratigraphy. *The geologic time scale* **1**, 127–144 (2012).  
 314
- [29] Gothmann, A. M. *et al.* Fossil corals as an archive of  
 315 secular variations in seawater chemistry since the mesozoic.  
 316 *Geochimica et Cosmochimica Acta* **160**, 188–208 (2015).  
 317
- [30] Bailey, T., McArthur, J., Prince, H. & Thirlwall, M. Disso-  
 318 lution methods for strontium isotope stratigraphy: whole  
 319 rock analysis. *Chemical Geology* **167**, 313–319 (2000).  
 320
- [31] Watanabe, T., Suzuki, A., Kawahata, H., Kan, H. & Ogawa,  
 321 S. A 60-year isotopic record from a mid-holocene fossil  
 322 giant clam (*Tridacna gigas*) in the ryukyu islands: physio-  
 323 logical and paleoclimatic implications. *Palaeogeography,*  
 324 *Palaeoclimatology, Palaeoecology* **212**, 343–354 (2004).  
 325